


Submitted: December 27, 2023

Revised: February 25, 2024

Accepted: March 10, 2024

Hybrid of a nonlinear Maxwell-type viscoelastoplastic model with the linear viscoelasticity constitutive equation and properties of crossbred creep and stress-strain curves

A.V. Khokhlov  1,2 ¹ Lomonosov Moscow State University, Moscow, Russia² North-Eastern Federal University, Yakutsk, Russia andrey-khokhlov@ya.ru

ABSTRACT

A generalization for the physically nonlinear Maxwell-type constitutive equation is proposed with two material functions for non-aging rheonomic materials, which have been studied analytically in previous articles to elucidate its properties and application. To extend the set of basic rheological phenomena that it simulates, we propose to add the third strain component expressed as the Boltzmann-Volterra linear integral operator governed by an arbitrary creep function. To generalize and conveniently tune the constitutive relation, to fit it to various materials and various lists of phenomena (test data), we introduce a weighting factor (i.e. nonlinearity factor) into the equation. This allows us to crossbred primary physically nonlinear Maxwell-type model with the linear viscoelasticity equation in an arbitrary proportion, to construct a hybrid model and to regulate prominence of different phenomena described by the two constitutive equations we crossbred. General expression for stress-strain curves at constant stress rate and for the creep and recovery curves families obtained using the proposed hybrid constitutive equation are derived and analyzed. The basic properties of the stress-strain curves and the creep-recovery curves are studied assuming three material functions are arbitrary. They are also compared to the properties obtained using primary Maxwell-type model and linear viscoelasticity theory. New properties are found that allow the hybrid model to tune the form of the stress-strain curves and the creep-recovery curves and to simulate additional effects observed in constant stress rate tests and creep-recovery tests of various materials at different stress rates and stress levels.

KEYWORDS

viscoplasticity • viscoelasticity • creep • physical non-linearity • material functions • stress-strain curves family stress rate sensitivity • equilibrium stress-strain curve • creep-recovery curves • applicability indicators

Acknowledgements. *The research was supported by the Russian Science Foundation grant No. 22-13-20056 "Development of resource-saving solid-phase technology for molding products and composite materials for the Arctic on the basis of polytetrafluoroethylene". Available online: <https://rscf.ru/project/22-13-20056/>.*

Citation: Khokhlov AV. Hybrid of a nonlinear Maxwell-type viscoelastoplastic model with the linear viscoelasticity constitutive equation and properties of crossbred creep and stress-strain curves *Materials Physics and Mechanics*. 2024; 52(4): 114–140.

http://dx.doi.org/10.18149/MPM.5242024_11

Introduction

The problem of reliable modeling of thermomechanical behavior and fracture of materials and structures, the issues of construction or selection of adequate constitutive equations (CEs) for viscoelastoplastic materials (out of dozens and hundreds proposed in the literature), analysis of their properties and the scope of application, sphere of influence of material functions (MFs) and phenomenological limitations on them, development of identification and certification techniques, still remain relevant in mechanics, materials

science and the practice of engineering calculations. For a reasonable choice of the CE, determination of its possibilities and the scope of application, for competent processing of experimental data and identification of MFs and parameters of the chosen CE it is necessary to study *analytically* general properties of loading and unloading curves, relaxation curves, creep curves under stepwise loading programs generated by the CE with *arbitrary* MFs [1–10]. It is also necessary to investigate the influence of loading parameters and characteristics of MFs, to identify the necessary conditions (indicators) of applicability of the CE to the modeled material.

In the series of papers [4–10] (and others) such an analysis was performed for a physically nonlinear CE:

$$\varepsilon(t) = E^{-1}F(\sigma(t)) + \eta^{-1} \int_0^t V(\sigma(\tau))d\tau, \text{ or } \dot{\varepsilon} = E^{-1}[F'(\sigma)\dot{\sigma} + \tau_r^{-1}V(\sigma)], t > 0, \quad (1)$$

connecting (in one-dimensional case) the strain $\varepsilon(t)$ with the history of stress changes $\sigma(\tau)$, $\tau \in [0; t]$, in isothermal deformation processes of stable rheonomic materials (stress and time are assume to be dimensionless). The CE (1) includes two increasing MFs $F(x)$, $V(x)$, $x \in (\omega_-, \omega_+)$ (their constraints are given in the next section) and two constants: $E, \eta > 0$. The elastic modulus E and the viscosity coefficient η are explicitly extracted from the MF to account for the effect of temperature in the form $E = E(T)$, $\eta = \eta(T)$ [5]. The CE (1) is based on the decomposition of the total strain into the sum of elastic and viscoplastic components: $\varepsilon = \varepsilon_e + \varepsilon_v$, $\varepsilon_e = F(\sigma)/E$, $\dot{\varepsilon}_v = V(\sigma)/\eta$.

It is aimed at describing a set of effects typical of non-aging materials with heredity and plasticity, high rate sensitivity and, possibly, tension-compression asymmetry. The CE (1) combines relative simplicity and wide scope of applicability: it generalizes a number of classical models (due to the arbitrariness of MFs $F(x)$ and $V(x)$) and describes a very wide range of rheological effects typical of many rheonomic materials exhibiting viscoelastic and plastic properties [4–10].

The CE (1) generalizes (includes) the classical power-law models of viscous flow and creep (see the surveys and the references on these topics in works [4,5,8]), the Herschel–Bulkley and Shvedov–Bingham rheological models, and the special case of the Sokolovsky–Malvern model. In the case of $F(x) \equiv 0$, $V(x) = x|x|^{n-1}$, $n > 1$, the CE (1) gives the power law of flow (Norton–Bailey model), the most popular (due to its simplicity) in the theory of creep, viscoplasticity, hydrodynamics of non-Newtonian fluids and the rheology of polymers [11–41]. It has been used to model the dependence of steady-state creep rate on stress [11–19,24,25,29], power-law fluid flows (in particular, those associated with oil production) [20–24], superplastic flow of materials [32–40], and the motion of avalanches and mudflows [41]. Setting $F(x) = x$ and $V(x) = x|x|^{n-1}$, we obtain a model with linear elasticity and power-law viscosity, which has been used in a number of works to describe the creep curves, to model superplasticity and to solve specific problems [8–10,13,34,42–45]. In [46,47], the CE, related to the CE (1), was used as the basis for a nonlinear model for describing the shear strain of thixotropic viscoelastic fluids, which takes into account the influence of the kinetics of formation and destruction of intermolecular bonds and associates of macromolecules on viscosity and shear modulus and the influence of the deformation process to this kinetics. The general tensor formulation of nonlinear Maxwell-type CEs for (severe strain of) viscoelastic media, related to the CE (1), the description of kinematics, thermodynamic aspects and

methods of specifying the CRs were studied in [48–53]. Those papers focused on describing the behavior of fluids and discussed experiments and effects inherent in fluids (polymer melts and solutions, etc.). However, they did not consider creep, relaxation and stress-strain curves generated by the CE, did not ask many questions specific to mechanics of deformable solids, and did not analyze the corresponding phenomenological constraints on the MFs and parameters of the CE (1) and methods for their identification. The CE (1) with arbitrary MFs $F(x)$ and $V(x)$ has not been systematically investigated and validated before the works [4–10].

Thus, the CE (1) generalizes several commonly used models and describes a wide range of rheological effects (see the next section and [4–10] for more details). However, along with many advantages, it has some features that limit its scope of applicability. Thus, the CE (1) is not capable of describing some effects observed during the deformation of many materials. For example, in [7,8] the following was proved:

1. the CE (1) models only creep at a constant rate (steady-state creep, characteristic of many ductile metals, polymers in a viscous-flow state and materials in a state of superplasticity) and is not capable of describing the stages of transient and accelerated creep, as well as limited creep, characteristic, for example, of many polymers;
2. the CE (1) does not describe recovery after complete unloading ("reverse creep", "elastic aftereffect"), i.e. the process of *gradual* relaxation of the accumulated strain reaching a certain constant level at large values of time, as it is observed in tests of many materials (for example, for cross-linked polymers and for bone tissue, reverse creep curves tend to the asymptote $\varepsilon = 0$). The CE (1) describes only the *instantaneous* recovery of the elastic part of strain. The "highly elastic" component of strain, which ensures gradual decrease, is completely absent in model (1);
3. under cyclic loading beyond the elastic limit, the CE (1) always gives ratcheting at a constant rate: "unlimited" increase in plastic strain without stabilization and adaptability, cyclic weakening.

Due to the abundance of advantages and possibilities of the CE (1), as well as the presence of several disadvantages, it is advisable to generalize the CE in such a way as to preserve the advantages, but eliminate the noted disadvantages and expand the range of rheological effects described by it and its scope of applicability. This is precisely the main purpose of this article (see the next sections).

The most important types of uniaxial tests, which make it possible to capture and examine various aspects of material behavior, to detect signs of nonlinearity in its behavior and to gather sufficiently rich information for the selection and identification of the CE, are the tests on loading (shear, tension, compression) at a constant rate $\sigma(t) = bt$ and on creep at a constant stress and recovery after unloading (reverse creep) [4,7,11–17,54–56] for different stress levels and durations of the loading stage $\bar{\sigma}, T > 0$, i.e. study of the response $\varepsilon(t; \bar{\sigma}, T)$ of a material (specimen) to a rectangular stress pulse: $\sigma(t; \bar{\sigma}, T) = \bar{\sigma}[h(t) - h(t - T)], t > 0$, (2) where $h(t)$ is the Heaviside function, instantaneous unloading and endurance at the $\sigma(t) = 0, t > T$.

Another objective of this article is to derive equations for the curves family and creep-recovery curves generated by the new CE (4) with three *arbitrary MFs* under loadings in the form (2). We also aim to study the influence of loading parameters and

characteristics of all MFs, in particular, to identify new qualitative properties (effects), which make it possible to describe a more general CE (4) in comparison with the CE (1). In the future, the properties found will be used to develop methods for identifying the CE (4) and searching for its applicability indicators using experimental creep and recovery curves of materials, as was done for the CE (1) in [4–10,56].

On restrictions on MFs of the CE (1) and its scope of applicability

The MF F defines in the CE (1) the elastic strain $\varepsilon_e(\sigma)$. The minimum primary constraints on it are: $F(x)$, $x \in (\omega_-, \omega_+)$ is a continuous (strictly) increasing function with a piecewise continuous derivative, such that $F(0) = 0$. These conditions ensure that the signs of stress and elastic strain $\varepsilon_e(\sigma)$ coincide and that the condition $\varepsilon_e(0) = 0$ is met. From the strictly increasing $F(x)$ it follows that $\varepsilon_e(|\sigma|)$ and the energy of elastic strain increase with increasing $|\sigma|$ and the existence of the inverse to F function f . The viscosity function $V(x)/\eta$ in the CE (1) controls the viscoplastic properties: it governs the material memory, the rate of dissipation, relaxation rate, creep and plastic strain accumulation rate, the sensitivity of stress (in particular, the instantaneous modulus and flow stress) to the strain rate, and the long-term strength [4–10]. The minimum constraints on it are: $V(x)$ is a continuous (non-strictly) increasing function on the interval (ω_-, ω_+) , such that $V(0) = 0$. These constraints on the MF provide, in particular, an increase in strain-stress curves and creep curves, a decrease in relaxation and long-term strength curves, a description of the complex of rheological effects typical of viscoelastoplastic materials (see below), and the thermodynamic consistency of the CR, i.e., the positivity of the stress work $\sigma(\tau)$ in an arbitrary deformation process and the non-negativity and increasing of dissipation $W[t, \sigma(\tau)]$: $\dot{W}(t) = \sigma(t)V(\sigma(t))/\eta > 0$. If ω_+ and ω_- are finite, they can be interpreted as tensile strength at tension and compression (as material parameters). Mathematical properties of the operator (1), literature reviews and related to (1) models used in the theory of creep, superplasticity and polymer mechanics, taking into account the effect of temperature and generalization of the CE (1) to the triaxial stress state are given in [4–10].

In [4–10] and others, were analytically studied the equations of the basic quasi-static curves families generated by the CE (1) with arbitrary MFs $F(x)$ and $V(x)$: relaxation and creep curves with arbitrary initial loading to a given level stage, creep under stepwise loading, long-term strength, stress-strain curves at constant and piecewise constant strain or loading rates, under cyclic loading. The general properties of these curves were studied depending on the characteristics of MFs and parameters of loading programs: intervals of monotonicity and convexity, inflection points, responses to discontinuities in the input process (jumps and breaks), asymptotics and two-sided estimates of theoretical curves, the nature of the convergence of their families to limit curves at the tendency of the parameters of loading programs (strain or loading rate, duration of the initial stage of loading, etc.) to zero and infinity, conditions for memory decay, the effect of permutation of loading stages on asymptotics and residual strain, etc. As a result of comparing the discovered properties of the theoretical curves with typical qualitative properties of test curves for a wide class of viscoelastoplastic materials (with a target list of mechanical effects), the necessary additional constraints on MFs were derived to

ensure adequate modeling of the main rheological effects, and theoretical and experimental applicability indicators of the CE (1) were identified, as well as those effects that it fundamentally cannot describe at any MFs.

A systematic study of the CE (1), carried out in a series of works [4–10] and others, showed that it can be used to describe a set of basic rheological effects typical of viscoelastoplastic materials with memory, high sensitivity to loading rate, and, possibly, tension-compression asymmetry. They are characterized by the following features of mechanical behavior:

1. increasing loading curves at a constant rate, which can be either convex upward or may have an inflection point;
2. positive rate sensitivity;
3. monotonous decrease and convexity of the unloading curve or the presence of a maximum point or inflection point on it (depending on the rate and level of loading),
4. lack of recovery (strain relaxation) after a stress pulse exceeding the elastic limit and complete unloading;
5. significant influence of the duration and rate of loading on the magnitude of plastic strain;
6. pronounced stage of flow at constant stress in stress-strain curves with constant rate and (increasing) dependence of the flow stress on rate;
7. "unlimited" increase in plastic strain under cyclic loading beyond the elastic limit (ratcheting without stabilization and adaptability, cyclic weakening);
8. creep at a constant rate;
9. stress relaxation to zero or non-zero value;
10. increase in compliance and rate sensitivity, an increase in the dissipation rate, relaxation rate, creep and ratcheting rates with increasing temperature.

Such materials (in certain deformation modes) include, for example, many polymers, their melts and solutions, solid fuels, asphalt concrete, high-modulus polyethylene yarns, geofabrics and geogrids, ice and frozen soils, titanium and aluminum alloys, carbon and ceramic materials at high temperatures, etc.

The analysis of the properties of theoretical curves generated by the CE (1) [4–10] showed that two main cases should be distinguish, in which the CE (1) (or the modeled material) behaves differently. In the first case, $|V(x)| > 0$ for all $x \neq 0$, 2) $V(x) \equiv 0$ at a certain interval $Z := [\sigma_-, \sigma_+] \subset (\omega_-, \omega_+)$, $\sigma_- \leq 0$, $\sigma_+ \geq 0$, $\sigma_+ \neq \sigma_-$ (by definition, σ_- and σ_+ are the lower and upper bounds of the set of zeros of the MF $V(x)$). In the second case, as long as $\sigma(t) \in Z$, the CE models the elastic behavior of the material: the dissipation is small and there is no hysteresis loop on the loading-unloading curve, the relaxation and creep are absent, the stress-strain curve does not depend on the loading (or strain) rate at $\varepsilon \in [\varepsilon_-, \varepsilon_+]$, where $\varepsilon_{\pm} := F(\sigma_{\pm})/E$. Thus, σ_- and σ_+ play the role of elastic limits (and creep thresholds) of the material under compression and tension. At $\sigma > \sigma_+$ (or $\sigma < \sigma_-$) the dissipation is significant and viscoplastic properties also begin to appear. For example, in [10], the elastic limit equal to one tenth of the tensile strength was found from the testing data of a complex polyester yarn and the methods of identification of the CE (1), developed in [8], were tested.

The use of a MF of the second kind, i.e. with $\sigma_+ > 0$, is very convenient for taking

into account the features of the manifestation of nonlinear viscoelastoplastic properties in testing data of a particular material, namely, for connecting the nonlinear viscoplasticity model (1) to the linear viscoplasticity CE (3) and surgical adjustment of this connection. Due to the material parameters σ_+ and w it is possible to add to the CE (3) the nonlinear viscoplasticity, starting from any stress $\sigma \geq \sigma_+ > 0$ and in any proportion.

Generalization of the CE (1) by crossbreeding with the linear viscoelasticity CE

A natural way to generalize the CE (1) in such a way as to preserve its advantages, but eliminate the noted disadvantages and expand the range of rheological effects described by it and its scope of applicability, is to add to the CE (1) a third strain component – viscoelastic, highly elastic strain, i.e., to sequentially attach to the nonlinear Maxwell-type model a linear viscoelastic element (a parallel connection is also promising, but will entail a distortion of the good properties already presented in the CE (1)): $\varepsilon = \varepsilon_e + \varepsilon_v + \varepsilon_{ve}$. This viscoelastic element can be chosen differently: a Scott-Blair fractal element can be added, Voigt or Kelvin models, etc. But it seems most reasonable to maximize the communication in this direction, i.e., to add a term governed not by two or three parameters, but expressed in general form by the linear Boltzmann-Volterra integral operator with an arbitrary creep function (CF):

$$\varepsilon(t) = \int_0^t \Pi(t - \tau) d\sigma(\tau), \sigma(t) = \int_0^t R(t - \tau) d\varepsilon(\tau), t \geq 0. \quad (3)$$

If, of course, it is possible to analyze in sufficient depth the properties of such a complex CE, depending on three arbitrary MFs, and to learn how to adjust these properties in order to describe typical material testing data. For generality and convenience of model control, its adjustment to different materials and lists of modeled effects, we introduce a weighting factor $w \in [0; 1]$ (nonlinearity factor), which allows us to “mix” the CE (1) and the linear viscoelasticity operator (3) (and the effects modeled by them) in any proportions:

$$\varepsilon(t) = wE^{-1}F(\sigma(t)) + w\eta^{-1} \int_0^t V(\sigma(\tau))d\tau + (1 - w) \int_0^t \Pi(t - \tau) d\sigma(\tau), t > 0. \quad (4)$$

Thus, the new CE (4) is a hybrid (and simultaneous generalization) of the nonlinear CE (1) and the linear viscoelasticity CE (3) (at $w = 0$, the nonlinearity is switched off and the linear viscoelasticity CE is obtained, and at $w = 1$ the CE (1) is obtained). It is the parameter w that allows us to adjust the contributions of the CE (1) and the CE (3) and thus to adjust the severity of the effects they model.

Further, we assume minimal constraints on the CF $\Pi(t), t > 0$, in the CE (4), inherited from the viscoelasticity CE (3) [1]: it is positive, differentiable, increasing and convex upward by $(0; \infty)$. For example, the following CF:

$$\Pi = At^u, u \in (0; 1), A > 0, \quad (5)$$

defines the so-called “fractal” element of “fractional” models with the fractional differentiation operator. It has the property $\Pi(0) = 0$, which characterizes irregular viscoelastic models (the corresponding relaxation function has a singularity at $t = 0$: $R(t) = Bt^{-u}$) [54]. The following CFs family:

$$\Pi(t) = \alpha t + \beta - \gamma e^{-\lambda t}, \lambda > 0, \alpha, \beta \geq 0, \gamma \in [0, \beta], \quad (6)$$

generates at $\gamma \in (0; \beta)$, $\alpha, \beta > 0$ all four regular structural models of four elements (they are equivalent), and at $\alpha = 0$ it generates two regular models of three elements (Kelvin and Poynting–Thomson models). Since $\Pi(0) = \beta - \gamma$, then the CF (6) generates irregular

models when $\gamma = \beta$: at $\lambda\beta = 0$ it is the Newtonian fluid, at $\alpha = 0$ it is the Voigt model, at $\alpha > 0$ it generates both singular models of three elements. At $\gamma = 0$ (6) it gives the linear Maxwell-type model. These CFs will be used to illustrate the properties of the creep and recovery curves generated by the CE (4). The case $\gamma < 0$ in (6) violates the constraint $\ddot{I}(t) \leq 0$, which entails an increase in the recovery curve (15) (a contradiction with experimental data).

The generalization of the CE (4) to the triaxial stress state in the case of isotropic media can be carried out according to the same standard scheme as the generalization of the CE (1), based on the postulate about the absence of cross-influence of the spherical and deviatoric parts of the stress and strain tensors $\boldsymbol{\sigma}(t)$ and $\boldsymbol{\varepsilon}(t)$ to each other (i.e., independence of volumetric strain from tangential stresses, and shear strains from average stress) and the postulate about the proportionality of deviators $\boldsymbol{s} = \boldsymbol{\sigma} - \sigma_0 \boldsymbol{I}$, $\boldsymbol{e} = \boldsymbol{\varepsilon} - \varepsilon_0 \boldsymbol{I}$ [9]:

$$\begin{aligned} \varepsilon_{ij}(t) &= \frac{3}{2} \varepsilon(t) \sigma(t)^{-1} s_{ij}(t) + \frac{1}{3} \theta(t) \delta_{ij}, \\ \boldsymbol{\varepsilon}(t) &= \boldsymbol{M} \boldsymbol{\sigma} = E^{-1} F(\boldsymbol{\sigma}(t)) + \eta^{-1} \int_0^t V(\boldsymbol{\sigma}(\tau)) d\tau, \end{aligned} \quad (7)$$

$$\boldsymbol{\theta}(t) = \boldsymbol{M}_0 \boldsymbol{\sigma}_0 = E_0^{-1} F_0(\boldsymbol{\sigma}_0(t)) + \eta_0^{-1} \int_0^t V_0(\boldsymbol{\sigma}_0(\tau)) d\tau,$$

where $\sigma_0(t) = \sigma_{ii}(t)/3$, $3\varepsilon_0 = \theta(t) = \varepsilon_{ii}(t)$, $\boldsymbol{\sigma}(t) = (\frac{3}{2} s_{ij} s_{ij})^{0.5}$, $\varepsilon(t) = (\frac{2}{3} e_{ij} e_{ij})^{0.5}$ are the average stress, volumetric strain and the intensity of stresses and strains. This CE expresses $\boldsymbol{\varepsilon}(t)$ through the history of $\boldsymbol{\sigma}(t)$ and is governed by two pairs of MFs $F(x)$, $V(x)$ and $F_0(x)$, $V_0(x)$, whose constraints are described in the previous section, and the parameters E , η , E_0 , $\eta_0 > 0$. The CE (7) can be crossbred according to the described scheme with the general linear viscoelasticity CE for isotropic media:

$$\varepsilon_{ij}(t) = e_{ij} + \varepsilon_0 \delta_{ij}, \quad e_{ij}(t) = \frac{3}{2} \boldsymbol{\Pi} s_{ij}(t), \quad \theta = \boldsymbol{\Pi}_0 \sigma_0, \quad (8)$$

$$\boldsymbol{\Pi} \boldsymbol{y} = \int_0^t \boldsymbol{\Pi}(t - \tau) d\boldsymbol{y}(\tau), \quad \boldsymbol{\Pi}_0 \boldsymbol{y} = \int_0^t \boldsymbol{\Pi}_0(t - \tau) d\boldsymbol{y}(\tau), \quad t > 0, \quad (9)$$

with two arbitrary MFs $\boldsymbol{\Pi}(t)$ and $\boldsymbol{\Pi}_0(t)$ (functions of shear and volumetric creep), i.e., consider the CE expressing $\boldsymbol{\varepsilon}(t)$ through the history of $\boldsymbol{\sigma}(t)$ as follows:

$$\begin{aligned} \varepsilon_{ij}(t) &= e_{ij}(t) + \frac{1}{3} \theta(t) \delta_{ij}, \\ e_{ij} &= \frac{3}{2} w \frac{M \boldsymbol{\sigma}}{\sigma(t)} s_{ij}(t) + \frac{3}{2} (1 - w) \boldsymbol{\Pi} s_{ij}(t), \end{aligned} \quad (10)$$

$$\theta = w \boldsymbol{M}_0 \sigma_0 + (1 - w) \boldsymbol{\Pi}_0 \sigma_0$$

The CE (10), like the CEs (7) and (8), describes the processes of isothermal deformation of non-aging isotropic viscoelastic media by connecting the histories of changes in the components of the deviators \boldsymbol{s} , \boldsymbol{e} and the first invariants $\sigma_0(t)$ and $\varepsilon_0(t)$ of the stress tensors $\boldsymbol{\sigma}(t)$ and small strains $\boldsymbol{\varepsilon}(t)$ at an arbitrary point of the body. The CE (10) contains six MFs: three governing the change in shape (F , V , $\boldsymbol{\Pi}$) and three governing the volumetric strain (or only one or two in the case of simplifications associated, for example, with the postulation of an elastic or linearly viscoelastic relation between the volumetric strain and the average stress).

A systematic study of the three-dimensional CE (10) and the study of the possibilities for modeling triaxial effects (in particular, the scenarios for changes in time of the transverse strain coefficient under creep and other types of loading, the influence of volumetric strain and hydrostatic pressure on the tension-compression curve [9,56]) – these are the topics of subsequent articles. The analysis should begin with the one-

dimensional operator (4). In the case of uniaxial (“pure”) shear, when only the components $\sigma_{12} = \sigma_{21}$ of the stress tensor are nonzero, there will be $\sigma_0(t) \equiv 0$, $\mathbf{s}(t) = \boldsymbol{\sigma}(t)$, and from the CE (10) it follows, that $\theta(t) \equiv 0$, $\mathbf{e}(t) = \boldsymbol{\varepsilon}(t)$, only the components $\varepsilon_{12} = \varepsilon_{21}$ are nonzero and they are connected to $\sigma_{12}(t)$ by an operator in the form (4). Therefore, all statements proved below about the creep and strain curves generated by the uniaxial CE (4) are automatically transferred to the CE (10) in the case of shear, as well as in the case of hydrostatic loading without shape change: for the volumetric creep curves $\theta(t, \bar{\sigma}_0)$ and loading curves $\sigma_0(\theta, b)$ families all properties are preserved when the triple of MFs F, V, Π are replaced by the MFs F_0, V_0, Π_0 .

Creep curves generated by the CE (1) and the CE (4)

At the stress $\boldsymbol{\sigma}(\mathbf{t}) = \bar{\boldsymbol{\sigma}} \mathbf{h}(\mathbf{t})$, $t > 0$, the CE (1) generates the creep curves family:

$$\boldsymbol{\varepsilon}(t, \bar{\boldsymbol{\sigma}}) = r(\bar{\boldsymbol{\sigma}})t + cF(\bar{\boldsymbol{\sigma}}), \text{ or } \boldsymbol{\varepsilon}(t, \bar{\boldsymbol{\sigma}}) = c[V(\bar{\boldsymbol{\sigma}})\tau_r^{-1}t + F(\bar{\boldsymbol{\sigma}})] \quad (11)$$

where $c = E^{-1}$, $r(\bar{\boldsymbol{\sigma}}) = \eta^{-1}V(\bar{\boldsymbol{\sigma}}) = c\tau_r^{-1}V(\bar{\boldsymbol{\sigma}})$, $\tau_r := \eta/E$ is the relaxation time of the linear Maxwell-type model with $V(x) = F(x) = x$ (τ_r is convenient to use for dimensionless time).

If $V(x) \equiv 0$ on a certain segment $[\sigma_-, \sigma_+]$, $\sigma_- < 0$, $\sigma_+ > 0$, then at $\sigma \in [\sigma_-, \sigma_+]$ the CE (1) models (nonlinearly) the elastic behavior of the material and at $\bar{\boldsymbol{\sigma}} \in [\sigma_-, \sigma_+]$ the creep is absent (the elastic limits for compression and tension coincide with the creep thresholds).

If $V(\bar{\boldsymbol{\sigma}}) \neq 0$, then all creep curves are linear in time at $t > 0$, i.e., for any MFs, the CE (1) models only creep at a constant rate (as does the linear Maxwell-type model), the rate $|r(\bar{\boldsymbol{\sigma}})|$ increases with the increase of $|\bar{\boldsymbol{\sigma}}|$. Since $V(\bar{\boldsymbol{\sigma}}) > 0$ at $\bar{\boldsymbol{\sigma}} > 0$ and increases, the creep curve (11) increases along t (at $\bar{\boldsymbol{\sigma}} > 0$) and along $\bar{\boldsymbol{\sigma}}$, which is observed in tests of stable materials.

A pronounced stage of creep at a constant rate is characteristic of many plastic metals, polymers in a viscous-flow state, and materials in a state of superplasticity. The creep curves of polymers have a stage of steady-state creep only at sufficiently high temperatures, when the polymer is in a viscous-flow state. The CE (1) is not capable of describing the stages of transient and accelerated creep, as well as limited creep, characteristic, for example, of many polymers.

For example, Fig. 1(a) shows the creep and recovery curves of 110×2Z50 complex polyester yarn under tension according to program (2), carried out in 2019 by O.N. Stolyarov and A.V. Khokhlov at the Peter the Great St. Petersburg Polytechnic University (on the Instron 5965 universal measuring complex). The basic characteristics of the yarn were measured beforehand. Linear density of the yarn $\theta = 220$ tex, specific density of the yarn material $\gamma = 1360$ kg/m³, elastic modulus 15.3 ± 1.1 GPa, breaking force $N_* = 150 \pm 5$ N (tensile strength $\sigma_* = 960 \pm 35$ MPa, relative strength of the yarn is 0.7 N/tex), relative elongation at break is 11 ± 0.75 % (based on the results of ten tests to break with a crosshead rate of 50 mm/min). Figure 1(a) shows creep and recovery curves of yarn specimens (the length of the working part of the specimen is 100 mm) for different stress levels: the curve i corresponds to the stress $\bar{\boldsymbol{\sigma}} = \bar{\boldsymbol{\sigma}}_i = i\sigma_*/10$ (from 10 to 50 % of the tensile strength). The ideal program (2) was implemented as follows: “instantaneous” loading (more precisely, very fast: within 1–3 sec, at a rate of

1500 N/min) of the specimen to a given stress level $\bar{\sigma}$, holding for a time $t_* = 4\tilde{t}$, $\tilde{t} = 3600$ sec (1 hour), "instantaneous" unloading and subsequent holding at (almost) zero stress (2 N) for a time of $2\tilde{t}$ to analyze the recovery process.

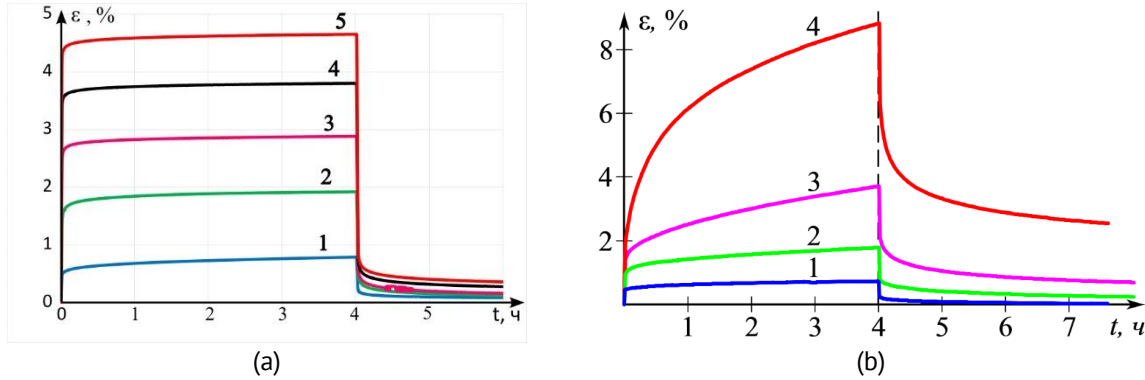


Fig. 1. Test creep and recovery curves at different tensile loads for a polyester yarn (a) and polyamide-6 (b)

The data of these tests the CE (1) approximates well except for the initial segments of the creep curve and the recovery stage. However, the data from tests of polyamide-6 under tension (Fig. 1(b)) the CE (1) cannot describe for the reasons mentioned above (creep at an unstable rate, pronounced reverse creep). S.B. Sapozhnikov at the South Ural State University (in August 2022) carried out these (preliminary) tests according to the following program. Rapid loading up to $\bar{\sigma} = \bar{\sigma}_i = 10; 20; 25; 30$ MPa, observation of creep at constant stress for 4 hours (curves 1–4), "instant" unloading and observation of recovery at (almost) zero stress for 4 hours. To select the stress levels, preliminary tests to failure were carried out at different loading rates and the conditional tensile strength of polyamide-6 was found in the range of loading rates from 0.5 to 50 MPa/min and $\sigma_* = 60 \pm 5$ MPa (true stress at the break $\sigma_* = 80 \pm 10$ MPa, relative elongation at break is from 20 to 50%). For polyamides and similar materials, the proposed CE (4) is useful.

Since the response of the linear CE (3) to the loading program $\sigma(t) = \bar{\sigma} h(t)$, has the form $\varepsilon(t, \bar{\sigma}) = \bar{\sigma} \Pi(t)$, then the CE (4) generates the creep curves family:

$$\varepsilon(t, \bar{\sigma}) = wr(\bar{\sigma})t + wcF(\bar{\sigma}) + (1 - w)\bar{\sigma}\Pi(t) \quad (12)$$

Since $w \in [0; 1]$, then the creep curves family (12) increases along $\bar{\sigma}$, which coincides with the typical properties of creep curves of structurally stable materials. At $\bar{\sigma} > 0$ the additional term $(1 - w)\bar{\sigma}\Pi(t)$ increases along t and is convex upward (since $\Pi(t)$ is increasing and convex upward). Therefore, the creep curve (12) *increases along t and is convex upward at $t > 0$* , as in linear viscoelasticity, but no longer depends linearly on the stress level $\bar{\sigma}$ (since the first two terms do not have this property). At $w > 0.5$ the influence of the first term on the creep rate and the accumulation of irreversible (residual) strain is significant, and it is possible to make the creep curve as close as desired to the straight-line creep curve (11) by increasing w . On the contrary, at $w \rightarrow 0$ it is possible to make the relative contribution of terms nonlinear along $\bar{\sigma}$ as small as desired and give the creep curves family any shapes characteristic of linear viscoelasticity. The convexity of the creep curve (12) means that the CE (4), like the linear viscoelasticity CR, is not capable of describing accelerated creep (the third stage of creep).

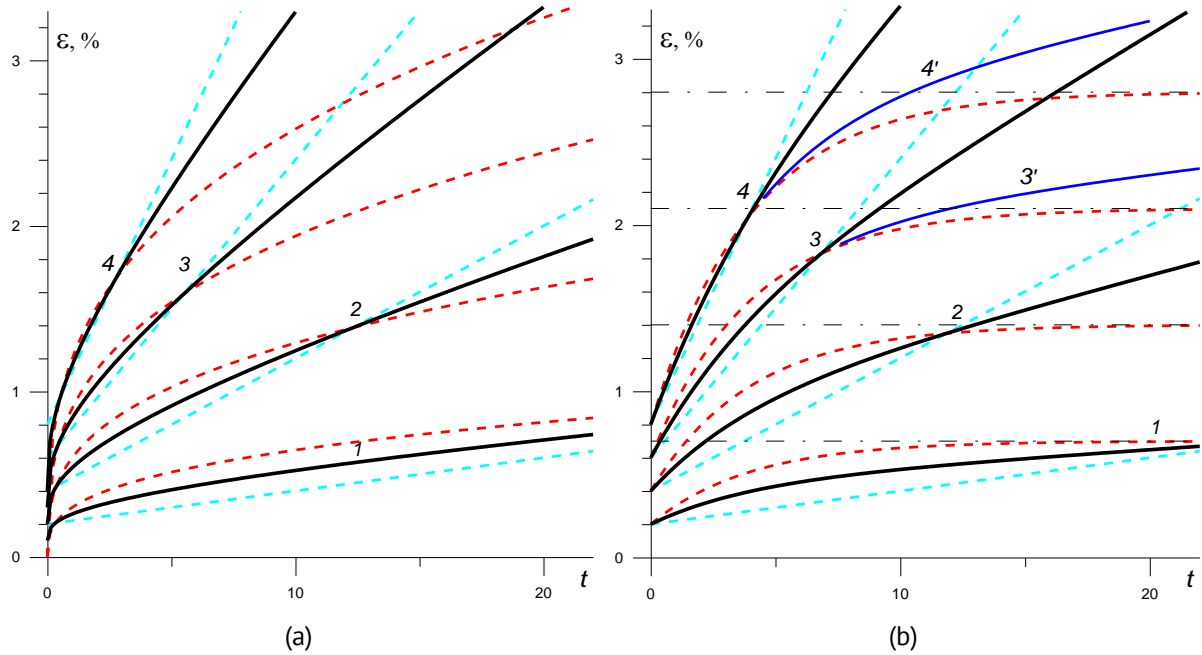


Fig. 2. Creep curves for four stress levels $\bar{\sigma} = 0.1; 0.2; 0.3; 0.4$ (curves 1–4), generated by several models of the form (4) with $F(x) = x, V(x) = x|x|, E = 50, \eta = 50$ and three different weighting factors $w = 0; 0.5; 1$ (red, black, and light blue curves): (a) three models with the creep function (5) with $u = 1/3, A = 0.03$; (b) three models with the creep function (6), $\alpha = 0, \beta = 0.07, \gamma = 0.05, \lambda = 0.25$

Figure 2(a) shows the creep curves of the three CE (4) with $F(x) = x, V(x) = x|x|, E = 50, \eta = 50$ (then $\tau_r = 1$), $\Pi = At^u, u = 1/3, A = 0.03$ with three different weighting factors $w = 0; 0.5; 1$ (red, black, and light blue curves) for four stress levels $\bar{\sigma} = 0.1; 0.2; 0.3; 0.4$ (curves 1–4). Dimensionless time is plotted along the abscissa axis: the considered qualitative properties of the curves do not depend on its scaling, $\bar{\sigma}$ and E are dimensionless by dividing by one tenth the quasi-static tensile strength at a standard rate. Since $\Pi(0) = 0$, the initial value of the creep curve $\varepsilon(0) = wcF(\bar{\sigma})$.

Figure 2(b) shows the creep curves of the three CE (4) with the same MFs $F(x) = x, V(x) = x|x|, E = 50, \eta = 50$ ($\tau_r = 1$) and three weighting factors $w = 0; 0.5; 1$ (red, black, and light blue curves) for the same $\bar{\sigma} = 0.1; 0.2; 0.3; 0.4$ (curves 1–4), but with a different CF: in the form (6) with $\alpha = 0, \beta = 0.07, \gamma = 0.05, \lambda = 0.25$. That is, to modify the CE (1) with the same MFs, the Kelvin model with retardation time $1/\lambda = 4 = 4\tau_r$ and relaxation time $(\beta - \gamma)/(\beta\lambda) = 8/7$ was used. Its CF is limited, $\Pi(\infty) = \beta$, the creep curves of this model (red lines) tend at $t \rightarrow \infty$ to asymptotes $\varepsilon = \bar{\sigma}\beta$. This example clearly shows how significantly the creep curves of the CE (4) differ from the creep curves of the CE (1) due to the introduction of an additional strain component (and the MF Π , that governs it). Obviously, changing the “hybridization” parameter $w \in [0; 1]$ provides a wide range of possibilities to adjust the shape of the creep curves of the CE (4) (Fig. 2(b) shows in blue the creep curves 3', 4', generated by the CR (4) with the same MFs, but with $w = 0.1$).

Creep and recovery curves

The creep and recovery curves, generated by the CE (1), are its responses to a rectangular stress pulse (2) with parameters $T > 0$, $\bar{\sigma} > \sigma_+ \geq 0$. Substituting Eq. (2) into Eq. (1) gives the equation for the creep and recovery curves family:

$$\varepsilon(t; \bar{\sigma}, T) = r(\bar{\sigma})t + cF(\bar{\sigma}) \text{ at } t < T, \quad \varepsilon(t; \bar{\sigma}, T) = p(\bar{\sigma}, T) \text{ at } t > T, \quad (13)$$

$$r(\bar{\sigma}) = \eta^{-1}V(\bar{\sigma}), \quad p(\bar{\sigma}, T) = \eta^{-1}V(\bar{\sigma})T = c\tau_r^{-1}V(\bar{\sigma})T. \quad (14)$$

The strain jump at the point $t = T$ is equal to $-cF(\bar{\sigma})$, $c = E^{-1}$, at $t > T$ the strain becomes constant and equal to the creep strain $p(\bar{\sigma}, T)$ accumulated over time T . At complete unloading, only the elastic strain $\varepsilon(+0) = cF(\bar{\sigma})$ disappears, and the entire accumulated creep strain turns out to be irreversible, plastic. This is precisely the behavior that many metals (and other materials) exhibit at sufficiently high temperatures. Thus, the CE (1) does not describe "reverse creep", i.e., the process of *gradual* relaxation of the accumulated strain to some constant level at large values of time, as is observed in tests of many materials. The CE (1) describes only the *instantaneous* recovery (the limiting, idealized case) of elastic strain. The "highly elastic" component of strain, which ensures gradual decrease, is completely absent in model (1). The residual strain $p(\bar{\sigma}, T)$ is proportional to the duration of the loading stage T , depends only on the MF V (as does the creep rate $r(\bar{\sigma})$) and increases with increasing $\bar{\sigma}$.

Due to (13), the trace left by a finite stress pulse (2) is never erased, i.e., the memory of model (1) is not fading, but is "permanent". The inability to describe materials with fading memory is a disadvantage of the CE (1), which narrows the range of modeled materials and processes.

However, this indicates that the CE (1) may be capable of describing not only viscoelasticity, but also viscoplasticity. This hypothesis is confirmed by the presence of horizontal asymptotes in the stress-strain curves generated by the CE (1) at a constant strain rate, horizontal asymptotes, i.e., flow segments at constant stress (without subsequent strengthening), as is observed in materials in a state of superplasticity [32-40] (they are characterized by creep at a constant rate and the absence of recovery after unloading).

The MF F does not affect the creep rate, its jumps and plastic strain $p(\bar{\sigma}, t_*)$, and V does not affect instant strain jumps. This allows to determine the MFs $\gamma V(x)$ and $F(x)/E$ separately based on the material creep and recovery curves [7].

The response of the linear CE (3) to a rectangular stress pulse (2) has the form: $\varepsilon(t) = \bar{\sigma}S(t; T)$, $S(t; T) := \Pi(t)h(t) - \Pi(t - T)h(t - T)$, $t > 0$.

At the point $t = T$ the creep and recovery curve $\varepsilon(t)$ has a jump $-\bar{\sigma}\Pi(0)$, and $\dot{\varepsilon}(t)$ has a jump $-\bar{\sigma}\dot{\Pi}(0)$. In the interval $t > T$ the equation of creep and recovery curves has the following form:

$$\varepsilon(t; \bar{\sigma}, T) = \bar{\sigma}S(t; T), \quad S(t; T) = \Pi(t) - \Pi(t - T), \quad t > T. \quad (15)$$

From the (non-strict) requirement that the recovery curve (15) decreases (with any T) it follows that $\dot{\Pi}(t)$ does not increase [54]. Therefore, a constraint should be imposed on the CF in the CE (1): $\Pi(t)$ has no downward convexity segments. Since $\dot{\Pi}(t)$ decreases on the ray $t > 0$ and $\dot{\Pi}(t) > 0$, there exists a limit $v := \dot{\Pi}(\infty) \geq 0$. Since the function (15) is decreasing and positive (bounded from below), it has at $t \rightarrow \infty$ a limit $\varepsilon_\infty \geq 0$, and $\varepsilon_\infty = \bar{\sigma}S(\infty, T)$. It is easy to prove that $S(\infty, T) = vT$ [54], i.e., in the case of $v > 0$ after

complete unloading (infinitely long), the residual strain $\varepsilon_\infty = \bar{\sigma}vT$ remains. This means that at $v > 0$, the memory of the integral operator Π , defining the CE (3), does not fade.

It can be proven that $v > 0$ for all regular structural models with even number of elements and all singular models with odd number of elements. If the CF is bounded (as for all regular structural models of an even number of elements), then $v = 0$ and $\varepsilon_\infty = 0$. It can also be $v = 0$ for an unbounded CF, for example, for a power-law CF $\Pi = At^u$, $u \in (0; 1), A > 0$. For models (6) $v = \alpha$ and $S(t; T) = \alpha T + \mu e^{-\lambda t}$, $\mu = \gamma(e^{\lambda T} - 1)$; in particular, $v > 0$ at $\alpha > 0$ (for the Maxwell-type model and its sequential connection with the Voigt model); for the Maxwell-type model and Newtonian fluid $\gamma = 0$ and $\varepsilon(t) = \bar{\sigma}\alpha T \equiv \text{const}$ at $t > T$, i.e. there is no recovery at all. For the Voigt (singular two-element model) and Kelvin (regular three-element model) models $\alpha = 0$, and therefore the creep and recovery curve (15) has the form $\varepsilon(t) = \bar{\sigma}\mu e^{-\lambda t}$, and $\varepsilon_\infty = 0$.

The creep and recovery curve of the CE (4) is obtained by combining the responses (13) and (15) of the CE (1) and the linear CE (3) to the stress pulse (2): at $t < T$ $\varepsilon(t; \bar{\sigma}, T)$ is given by equation (12), and at $t > T$:

$$\varepsilon(t; \bar{\sigma}, T) = wp(\bar{\sigma}, T) + (1 - w)\bar{\sigma}S(t; T), S(t; T) = \Pi(t) - \Pi(t - T), t > T. \quad (16)$$

Obviously, both terms (16) increase in absolute value with increasing $|\bar{\sigma}|$, and $|\varepsilon(t; \bar{\sigma}, T)|$ increases along $|\bar{\sigma}|$ and decreases along t at $t > T$ (since $S(t; T)$ decreases). These properties reflect typical qualitative properties of creep and recovery curves of structurally stable materials, i.e., the CE (4) adequately describes the recovery effect, in contrast to the CE (1). At $t \rightarrow \infty$ there is a limit (residual strain, horizontal asymptote for (16)):

$$\varepsilon_\infty(\bar{\sigma}, T) = wp(\bar{\sigma}, T) + (1 - w)\bar{\sigma}vT = w\eta^{-1}V(\bar{\sigma})T + (1 - w)\bar{\sigma}vT, v := \dot{\Pi}(\infty) \geq 0. \quad (17)$$

It is proportional to the duration of the loading stage T (this is one of the applicability indicators of the CE (4)), does not depend on the MF F and increases with increasing $\bar{\sigma}$. If the CF is chosen so that $v = 0$, then the residual strain (16) can be made as small as desired by decreasing the parameter w , and thus “remove” the residual strain given by the CE (1), if the CE is adjusted to the testing data of a specific material requires this.

At the point $t = T$ the creep and recovery curve (12), (16) has a jump $-wcF(\bar{\sigma}) - (1 - w)\Pi(0)\bar{\sigma}$. It is equal in absolute value to the jump $\varepsilon(0+; \bar{\sigma}, T) = wcF(\bar{\sigma}) + (1 - w)\Pi(0)\bar{\sigma}$ at the point $t = 0$. The equality of these jumps is another applicability indicator of the CE (4): this property is not always satisfied in material tests. If $\Pi(0) = 0$ (such linear models are called irregular, they have many specific properties [54]; these include, in particular, the Voigt model, the fractal element and all their successive connections), then the creep and recovery curve (15) is continuous at the point $t = T$, and the jump of the creep and recovery curve (12), (16) is equal to $-wcF(\bar{\sigma})$ and it can be made as small as desired by decreasing w .

Figure 3(a) shows the creep and recovery curves of three CE (4) with $F(x) = x$, $V(x) = x|x|$, $E = 50$, $\eta = 50$ (then $\tau_r = 1$), the CF (5) with $u = 1/3$, $A = 0.03$ and three weighting factors $w = 0; 0.5; 1$ (red, black and light blue curves) for loadings (2) with $T = 10$ and three stresses $\bar{\sigma} = 0.1; 0.2; 0.3$ (curves 1–3). Since $\Pi(0) = 0$, the creep and recovery curves of the (linear) CE with $w = 0$ are continuous at the point $t = T$ and the jump of any creep and recovery curve of the model with $w = 0.5$ (black curves) is half the jump of the creep and recovery curve of the model with $w = 1$ (i.e. model (1)) for the same $\bar{\sigma}$. Since $v = \dot{\Pi}(\infty) = 0$, for all creep and recovery curves the (linear) CE with $w = 0$, $\varepsilon_\infty(\bar{\sigma}, T) = 0$, i.e. they converge at $t \rightarrow \infty$ to a common asymptote $\varepsilon = 0$.

Therefore, the residual strain $\varepsilon_\infty(\bar{\sigma}, T)$ of the model with $w = 0.5$ is two times smaller than that of the model (1) (the asymptotes of curves 1–3 are shown as dash-dotted straight lines), and the recovery is slow (in comparison, for example, with Fig. 3(b)). This example clearly shows how significantly different the creep and recovery curves of the CE (4) are from the creep and recovery curves of the CE (1) due to the introduction of an additional strain component (and the MF Π , that controls it).

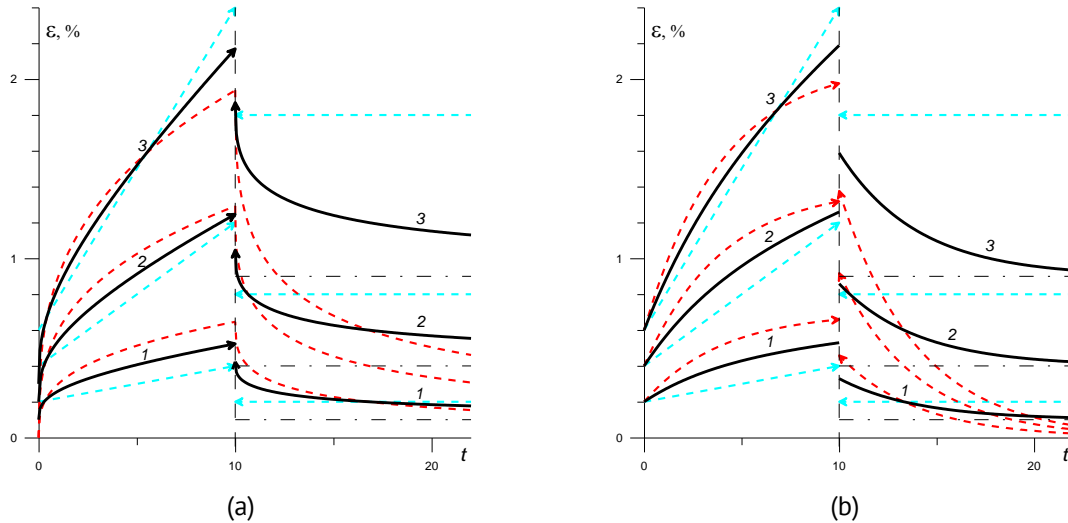


Fig. 3. Creep and recovery curves for three stress levels $\bar{\sigma} = 0.1; 0.2; 0.3$ (curves 1–3) generated by several models of the form (4) with $F(x) = x, V(x) = x|x|, E = 50, \eta = 50$ and three different weighting factors $w = 0; 0.5; 1$ (red, black, and light blue curves): (a) three models with the creep function (5) with $u = 1/3, A = 0.03$; (b) three models with the creep function (6) with $\alpha = 0, \beta = 0.07, \gamma = 0.05, \lambda = 0.25$

Figure 3(b) shows the creep and recovery curves of three CR (4) with the same MFs $F(x) = x, V(x) = x|x|, E = 50, \eta = 50$ ($\tau_r = 1$) with three different weighting factors $w = 0; 0.5; 1$ (red, black and light blue curves) for loadings (2) with $T = 10$ and three stress levels $\bar{\sigma} = 0.1; 0.2; 0.3$ (curves 1–3), but with a different CF: in the form (6) with $\alpha = 0, \beta = 0.07, \gamma = 0.05, \lambda = 0.25$. That is, to modify the CE (1) with the same MFs, the Kelvin model with retardation time $1/\lambda = 4 = 4\tau_r$ is used; its CF is limited, $\Pi(\infty) = \beta, \Pi(0) = \beta - \gamma, S(t; T) = \gamma(e^{\lambda T} - 1)e^{-\lambda t}$ and the creep and recovery curves of this model (red lines) have jumps $\Pi(0)\bar{\sigma} = (\beta - \gamma)\bar{\sigma}$ at the points $t = 0$ and $t = T$, and at $t \rightarrow \infty$ they tend to common asymptote $\varepsilon = 0$ (for any material parameters and any $\bar{\sigma}$, since $\varepsilon_\infty = \bar{\sigma}vT = 0$) with a rate $e^{-\lambda t}$ (much faster than the model in Fig. 3(a)).

It should be noted that the results of this section allow us to derive the equation of creep curves of the CE (4) under arbitrary stepwise loading (with any number of stress stages) by analogy with those obtained in articles [4,7,54].

General properties of stress-strain curves generated by the linear viscoelasticity CE

The loading $\sigma(t) = bt$ at a constant rate $b > 0$ (for definiteness, we consider the case $b > 0$), the linear CE (3) maps into following strain: $\varepsilon(t, b) = bQ(t) = bt\theta(t), Q(t) = \int_0^t \Pi(\tau) d\tau, \theta(t) = t^{-1}Q(t), t > 0$.

Excluding the parameter t gives the loading curves generated by the CE (3) under loading $\sigma(t) = bt$:

$$\varepsilon(\sigma, b) = bQ(\sigma/b) = \Theta(\sigma/b)\sigma, \sigma \geq 0. \quad (18)$$

The properties of averaging $\theta(t)$ are similar to the properties of the CF [55, 56]: $\theta(t)$ is an increasing smooth function at $t > 0$, $\Pi(t)/2 < \theta(t) < \Pi(t/2) < \Pi(t)$ (since $\Pi(t)$ is increasing and convex upward), $\theta(0+) = \Pi(0)$, $\theta(\infty) = \Pi(\infty)$, $\dot{\theta}(0+) = \dot{\Pi}(0+)/2$, and Q has the following properties: $Q(0) = 0$, $Q(\infty) = \infty$, $\dot{Q}(t) = \Pi(t) > 0$, $\ddot{Q}(t) = \dot{\Pi}(t) > 0$, $\ddot{Q}(t) = \ddot{\Pi}(t) \leq 0$ и $0.5(\Pi(t) + \Pi(0)) < Q(t)/t < \Pi(t/2) < \Pi(t)$, $t > 0$.

To obtain the equations of loading curves (18) in the form $\sigma = \sigma(\varepsilon, b)$, it is necessary to introduce into consideration the function $P(x)$, $x > 0$ inverse to the increasing function Q :

$$\sigma(\varepsilon, b) = bP(\varepsilon/b), \varepsilon, b > 0. \quad (19)$$

From the positivity and increase of the CF, it follows that P is an increasing upward convex function, $P(0) = 0$, $P(\infty) = \infty$, $P'(0+) = 1/\Pi(0)$ (in particular, $P'(0+) = \infty$, if $\Pi(0) = 0$), $P'(\infty) = 1/\Pi(\infty)$, the function $P(x)/x$ is decreasing and $P(x)/x > P'(x)$ at $x > 0$ [3]. From the constraints $\dot{\Pi} > 0$ and $\ddot{\Pi} \leq 0$ on the CF and the properties of the functions Q and P , the following general properties of the loading curves (19) follow.

The tangent and secant moduli of the stress-strain curves (19) are: $\sigma'_\varepsilon(\varepsilon, b) = 1/\varepsilon'_\sigma(\sigma, b) = 1/\Pi(\sigma/b)$ and $\sigma/\varepsilon = 1/\theta(\sigma/b)$ (since the uniaxial CE (3) coincides with the linear viscoelasticity CE for the components of the deviators of the stress and strain tensors, they can be considered shear moduli, although similar properties can be derived for loading curves in tension or compression [56]). Since $\varepsilon'_\sigma(\sigma, b) > 0$ and $\sigma'_\varepsilon > 0$, any loading curve (18) increases along σ , and the loading curve $\sigma = \sigma(\varepsilon, b)$ increases along ε at any b . Since the CF increases, $\varepsilon'_\sigma(\sigma, b)$ increases along σ and decreases along b , and $\sigma'_\varepsilon(\varepsilon, b)$ decreases along ε and increases along b . Therefore, for any $b > 0$ the loading curves (18) are convex downward, and the loading curves in the form (19) are convex upward on the semi-axis $\varepsilon > 0$. The upward convexity of the loading curve up to the beginning of fracture or to the yield point is characteristic of many polymers, asphalt concretes, metals and alloys [11,18,19,24,27,28,32–34].

The stress-strain curves family (18) decreases along b , since $\dot{\theta}(t) > 0$ and $\theta(\sigma/b)$ decreases along b , and the loading curves family in the form (19) increases along b (the higher the rate, the higher lies the loading curve $\sigma = \sigma(\varepsilon, b)$), i.e. the CE (3) models only positive rate sensitivity.

The stress-strain curve (18) depends on b , but the instantaneous modulus (shear modulus G or volumetric modulus K) does not depend on the loading rate: $G := \sigma'_\varepsilon(0, b) = \Pi(0)^{-1}$ (for models with $\Pi(0) = 0$ it will be $G = \infty$). At $\varepsilon \rightarrow \infty$ the tangent and secant moduli tend to the common limit $G_\infty = R(\infty) = 1/\Pi(\infty) \geq 0$ (if the CF is limited, then $G_\infty > 0$; if the CF is not limited, then $G_\infty = 0$). Thus, the long-term modulus G_∞ also does not depend on the loading rate.

Any stress-strain curve (18) lies "above" (along the ε axis) the straight line $\varepsilon = \Pi(0)\sigma$, since $\theta(t) > \theta(0+) = \Pi(0)$, and all the stress-strain curves in the form $\sigma(\varepsilon, b)$ lie below (along the σ axis) this straight line. More precisely, in the case of $\Pi(0) \neq 0$ (for regular models), two-sided estimates are valid for all loading curves (18) and (19): $\Pi(0)\sigma < \varepsilon(\sigma; b) < \Pi(\infty)\sigma$, $G_\infty\varepsilon < \sigma(\varepsilon, b) < G\varepsilon$. (20)

At $b \rightarrow +\infty$ the stress-strain curves family $\varepsilon(\sigma; b)$ of any regular model converges from above (and the family $\sigma(\varepsilon, b)$ from below) to the straight line $\varepsilon = \sigma/G$ uniformly on any segment of

the σ axis [55]: $\sup_{[0,\omega]} |\varepsilon - \sigma/G| = \sup_{[0,\omega]} \sigma |\theta(\sigma/b) - \Pi(0)| = \omega |\theta(\omega/b) - \Pi(0)| \rightarrow 0$, since $\dot{\theta}(t) > 0$ and $\theta(0+) = \Pi(0)$. Therefore, the straight line $\sigma = G\varepsilon$ is the instant loading curve of the CE (3) in the case of $\Pi(0) \neq 0$. The stress-strain curves family at a constant strain rate also converges to it [55]. If $\Pi(0) = 0$ (as in the CF (5)), then $G = \infty$, the tangent to any loading curve (18) at zero is horizontal, and the tangent to the loading curve in the form (19) is vertical, and the loading curves family (18) uniformly converges at $b \rightarrow +\infty$ to the straight line $\varepsilon = 0$.

At $b \rightarrow 0$ the stress-strain curves family (18) always converges (from above) to the straight line $\sigma = G_\infty \varepsilon$ (equilibrium loading curve) uniformly on any segment of the semi-axis $\varepsilon > 0$. This is also true in the case of unbounded or singular relaxation functions.

The stress-strain curve (18) has an asymptote at $\sigma \rightarrow \infty$ only when the CF is limited and the integral $Y := \int_0^{+\infty} [\Pi(\infty) - \Pi(\tau)] d\tau$ converges (obviously, $Y > 0$) [55], its equation: $\varepsilon = \Pi(\infty)\sigma - bY$, or $\sigma = G_\infty(\varepsilon + Yb)$. All the stress-strain curves $\sigma(\varepsilon, b)$ tend to an asymptote from below. Its angular coefficient is equal to the long-term modulus G_∞ and does not depend on b . The question of the existence of asymptotes for the stress-strain curves is not purely abstract, since reaching an asymptote (straightening of stress-strain curves, "linear hardening" mode) can occur in the operating range of strains and stresses.

For example, for models (6) $Q = 0.5\alpha t^2 + \beta t - \gamma\lambda^{-1}(1 - e^{-\lambda t})$, and the stress-strain curves family (18) has the following form:

$$\varepsilon(\sigma, b) = 0.5\alpha b^{-1}\sigma^2 + \beta\sigma - \gamma\lambda^{-1}b(1 - e^{-\lambda\sigma/b}), \sigma > 0. \quad (21)$$

The instantaneous modulus $G = 1/(\beta - \gamma)$; for models with $\gamma = \beta$ (singular) $G = \infty$. If $\alpha = 0$, i.e., for Voigt (with $\gamma = \beta$) and Kelvin ($\gamma \in (0; \beta)$) models, then $\Pi(\infty) = \beta < \infty$, $Y = \gamma/\lambda$, $G_\infty = 1/\beta$, and each loading curve has an asymptote $\sigma = \beta^{-1}(\varepsilon + \gamma\lambda^{-1}b)$ at $\varepsilon \rightarrow \infty$. If $\alpha > 0$, then $\Pi(\infty) = \infty$ and the loading curve (21) have no asymptotes. For the Maxwell-type model (the CF (6) with $\gamma = 0$, $\alpha, \beta > 0$) $G = 1/\beta$, $G_\infty = 0$ and the loading curves family converges at $b \rightarrow 0$ to the function $\sigma = 0$.

Figure 4(a) shows the stress-strain curves (21) of the Kelvin model (the CF (6) with $\alpha = 0$) at $\lambda = 0.1, \beta = 1, \gamma = 0.9$ (then $\Pi(0) = \beta - \gamma, G = 1/(\beta - \gamma) = 10, G_\infty = 1/\beta = 1$, retardation time $\tau = 1/\lambda = 10$, relaxation time $\tau_r = (1 - \gamma/\beta)\tau = 0.1\tau$) for the rates $b = 0.001; 0.01; 0.1; 1$ (black loading curves 1-4). Each loading curve $\sigma(\varepsilon, b)$ at $\varepsilon \rightarrow \infty$ has an asymptote $\sigma = G_\infty(\varepsilon + \gamma\tau b)$. The dash-dotted red straight lines 0 and ∞ are the instantaneous and equilibrium stress-strain curves $\sigma = G\varepsilon$ and $\sigma = G_\infty\varepsilon$, appearing in estimate (20); the family of loading curves of Kelvin model with any value of λ converges to them at $b \rightarrow \infty$ and $b \rightarrow 0$. For comparison, the stress-strain curves (21) of the Voigt model with $\gamma = \beta = 1$, the same $\lambda = 0.1$ and retardation time $\tau = 10$ (blue dashed loading curves 1''-4'') are given. For it, $\Pi(0) = 0$ (and the model is singular, since the relaxation function contains the term $\eta\delta(t)$ with the delta-function), $G = \infty$, $G_\infty = 1/\beta = 1$, the equilibrium loading curve $\sigma = G_\infty\varepsilon$ coincides with the straight line 0, at $b \rightarrow \infty$ the family $\varepsilon(\sigma, b)$ converges to $\varepsilon = 0$, and the loading curves $\sigma(\varepsilon, b)$ converge to the vertical semi-axis (i.e. the instantaneous loading curve does not exist). Each stress-strain curve at $\varepsilon \rightarrow \infty$ has an asymptote $\sigma = G_\infty\varepsilon + \tau b$, parallel to the equilibrium loading curve 0. The light blue curves 1'-4' are the loading curves (21) of the Maxwell-type model (i.e., the model with the CF (6) with $\gamma = 0$) with $\alpha = 1, \beta = 1$ for the same rates. Like Voigt model

it depends on two material parameters, but is regular: $\Pi(0) = \beta$, $G = 1/\beta = 1$, $\Pi(\infty) = \infty$, $G_\infty = 0$, relaxation time $\tau_r = \beta/\alpha = 1$. The stress-strain curves of the Maxwell-type model have no asymptotes. At $b \rightarrow 0$ and $b \rightarrow \infty$ the loading curves family $\sigma(\varepsilon, b)$ converges to the straight lines $\sigma = 0$ and $\sigma = G\varepsilon$ (the straight line 0). The light blue dashed curves $\underline{2}'$ - $\underline{4}'$ are the stress-strain curves of Maxwell-type model with the same instantaneous modulus $G = 10$, as the stress-strain curves 1-4 of the Kelvin model, i.e., the Maxwell-type model with $\beta = 0.1$, $\alpha = 1$. Therefore, its instantaneous loading curve coincides with the curve ∞ . The curve $1'''$ is the loading curve of the fractal model (5) with $u = 0.3$ for $b = 0.1$, i.e., exactly the stress-strain curve 3 from Fig. 4(b).

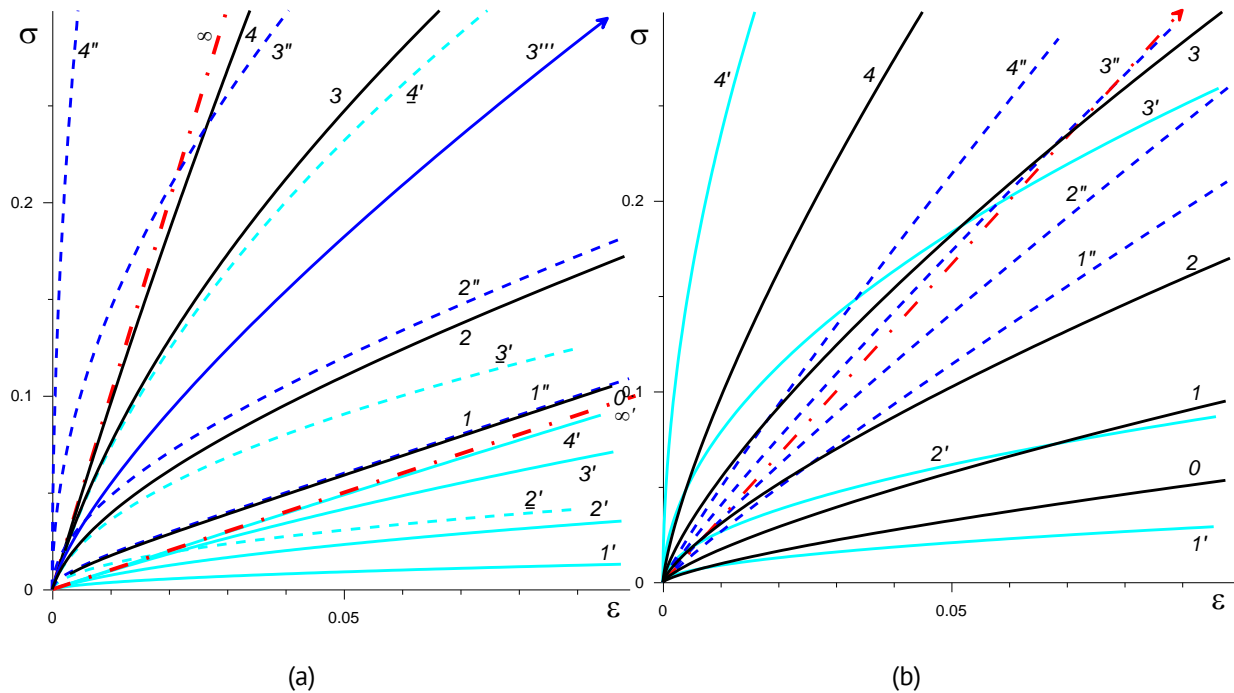


Fig. 4. (a) Stress-strain curves (21) generated by the classic Kelvin-Voigt, Maxwell and standard linear solid models (blue, light blue, and black curves) at four stress rates $b = 0.001; 0.01; 0.1; 1$ (curves 1-4, 1'-4', 1''-4''); (b) stress-strain curves (22) generated by three models of the form (5) with $u = 0.3; 0.9; 0.1$ (black, light blue, and blue curves) at stress rates $b = 0.001; 0.01; 0.1; 1$ (curves 1-4, 1'-4', 1''-4')

Let us consider the loading curves of a fractal element, i.e., the model with a power-law CF (5) (it corresponds to an unlimited unbounded relaxation function $R(t) = A^{-1}C(u)t^{-u}$, $C(u) = (u\pi)^{-1} \sin u \pi$ [55]). For the CF (5) $\Pi(0) = 0$ (the model is irregular), $\Pi(\infty) = \infty$, $\theta = A(u + 1)^{-1}t^u$, and the equation of loading curves (18) has the following form:

$$\varepsilon(\sigma, b) = A(u + 1)^{-1} \sigma(\sigma/b)^u, \text{ or } \sigma(\varepsilon, b) = [(u + 1)A^{-1}b^{-1}\varepsilon]^{1/(u+1)}b. \quad (22)$$

$G = \infty$, $G_\infty = 0$, at $\varepsilon \rightarrow \infty$ the loading curves have no asymptote. At $b \rightarrow 0$ the loading curves family $\sigma(\varepsilon, b)$ converges to the function $\sigma = 0$, and at $b \rightarrow \infty$ the family $\varepsilon(\sigma, b)$ converges to $\varepsilon = 0$, i.e., the loading curves $\sigma(\varepsilon, b)$ converge to the semi-axis, the segment in the estimate (20) turns into the first quadrant.

Figure 4(b) shows the curves (22) of three models of the form (5) with $A = 0.3$ and $u = 0.3; 0.9; 0.1$ (black, light blue and blue dashed curves) for loading rates

$b = 0.001; 0.01; 0.1; 1$ (loading curves 1–4, 1'–4', 1''–4''). An additional curve 0 is for $b = 0.0001$. As u increases, the tangent modulus in the vicinity of zero increases, and the loading curves (22) become increasingly higher. At small u , the model becomes much less sensitive to rate: the curves straighten and come closer (loading curves 1''–4''), the fan opening angle quickly decreases, and at $u \rightarrow 0$ it contracts into a straight line $\sigma = A^{-1}\varepsilon$ (red dash-dotted line).

Properties of stress-strain curves with constant rate generated by the CE (1)

The loading $\sigma(t) = bt$ at a constant rate $b > 0$ CE (1) maps into the strain: $\varepsilon(t; b) = E^{-1}F(bt) + \eta^{-1} \int_0^t V(b\tau) d\tau = E^{-1}[F(bt) + (\tau_r b)^{-1}I(bt)]$, $I(s) = \int_0^s V(x) dx$, $\tau_r = \eta/E$.

Excluding the time $t = \sigma/b$, we obtain the stress-strain curves equation:

$$\varepsilon(\sigma, b) = E^{-1}[F(\sigma) + (\tau_r b)^{-1}I(\sigma)], \quad b, \sigma > 0. \quad (23)$$

If $\sigma_+ > 0$ (i.e., $V(x) \equiv 0$ at $x \in [0; \sigma_+]$), then at $\sigma < \sigma_+$ $I(\sigma) \equiv 0$, and therefore the stress-strain curve (23) has the form $\varepsilon(\sigma, b) = F(\sigma)/E$, i.e., the CE describes the behavior of a nonlinearly elastic material and the stress-strain curve does not depend on the loading rate at $\sigma < \sigma_+$. If $\sigma > \sigma_+$ (in particular, in the case of $\sigma_+ = 0$), then $V(x) > 0$ and $I(\sigma) > 0$, and therefore the stress-strain curve depends on the rate b : the loading curves family (23) decreases along b at $\sigma > \sigma_+$, and the loading curves family in the inverse form $\sigma = \sigma(\varepsilon, b)$ increases along b at $\varepsilon \geq \varepsilon_+$, where $\varepsilon_+ := F(\sigma_+)/E$ (the higher the loading rate, the higher lies the stress-strain curve $\sigma = \sigma(\varepsilon, b)$). For the strain (23), the estimate from below $\varepsilon(\sigma, b) \geq E^{-1}F(\sigma)$ at $b, \sigma > 0$ is valid (if $\sigma > \sigma_+$, then the inequality is strict), and therefore for loading curves in the form $\sigma(\varepsilon, b)$ for all $b, \varepsilon > 0$ the estimate from above $\sigma(\varepsilon, b) \leq f(E\varepsilon)$ is true, where $f = F^{-1}$ is the inverse function of F . At $\varepsilon > \varepsilon_+$ this estimate can be refined:

$$\sigma_+ < \sigma(\varepsilon, b) < f(E\varepsilon), \quad \varepsilon > \varepsilon_+ \quad (24)$$

(in the case of $\sigma_+ = 0$ it is true for all $\varepsilon > 0$, and in the case of $\sigma_+ > 0$ $\sigma(\varepsilon, b) = f(E\varepsilon)$ at $\varepsilon \leq \varepsilon_+$).

The MF $I(s)$ increases and is convex downward at $\sigma > \sigma_+$, since $I''(s) = V'(s) > 0$. Therefore, all loading curves (23) increase along σ and the loading curves $\sigma = \sigma(\varepsilon, b)$ increase along ε , and if $F''(x) \geq 0$, then $\varepsilon''(\sigma) > 0$, the loading curves (23) are convex downward, and the loading curves $\sigma = \sigma(\varepsilon)$ are convex upward for any b .

As a result of analyzing the implicit representation of the loading curves (23) under the above mentioned minimum constraints on the two MF in [8], other basic properties of the loading curves $\sigma = \sigma(\varepsilon, b)$, $b > 0$ were found. Many properties of the loading curves of the nonlinear CE (1) are similar to the properties of the loading curves of the linear integral viscoelasticity CE. In particular, the CE (1) is also unable to describe the negative rate sensitivity [57–60] and the behavior of materials for which the dependence of the instantaneous modulus on the loading rate or strain has been reliably established: polymers at sufficiently high temperatures, copper, tin, aluminum, titanium alloys in the superplasticity regime, etc. [8,32–40,61–64]. Polymers in the glassy state and many other materials do not exhibit rate sensitivity at sufficiently small strains. This effect can be described only by replacing the instantaneous modulus with a secant modulus or one averaged in the vicinity of zero. These properties are the inapplicability indicators of the

CE (1), along with its inability to model creep at a variable rate, fading memory, recovery after unloading, the Mullins effect, and adaptability under soft asymmetrical cyclic loading [4–10]. But, in contrast to the loading curves of the linear CE, which are always convex upward, the loading curves of the CE (1) can (if $F''(x) < 0$) have inflection points and convexity downward on a certain interval $\varepsilon < \tilde{\varepsilon}(b)$, (at sufficiently small strain, as in many elastomers, foams, and biological tissues: ligaments, tendons, vessels [18,65–69]).

There are several other features of the loading curves of the CE (1) in comparison with the loading curves of the linear CE:

1. the dependence of the loading curve of the CE (1) on the loading rate b is monotonic, but nonlinear and can be different under tension and compression;
2. the tangent modulus of the loading curves $\partial\sigma/\partial\varepsilon = E[F'(\sigma) + (\tau_r b)^{-1}V(\sigma)]^{-1}$ depends on the rate (increases along b), but instantaneous moduli in tension and compression $E_{\pm} = E/F'(0\pm)$ (limit values of the tangent modulus of the loading curves at $\varepsilon \rightarrow 0 \pm 0$) do not depend on the rate b and the MF V , and can be different;
3. the instantaneous and equilibrium loading curves of the CE (1) (the limits of the loading curves family $\sigma(\varepsilon, b)$ at $b \rightarrow 0+$ and at $b \rightarrow \infty$) are no longer necessarily rectilinear: at $b \rightarrow \infty$ the loading curves family $\sigma(\varepsilon, b)$ converges on the ray $\varepsilon \geq 0$ to the curve $\sigma = f(E\varepsilon)$, $f = F^{-1}$ (curve ∞ in Fig. 5) uniformly on any segment of the axis ε . And at $b \rightarrow 0+$ the loading curves family $\sigma(\varepsilon, b)$ converges to the constant $\sigma = \sigma_+$ on the ray $\varepsilon \geq \varepsilon_+$ (curve 0 in Fig. 5), where $\varepsilon_+ := F(\sigma_+)/E$. And at $\varepsilon \in [0; \varepsilon_+]$ it converges to the function $\sigma = f(E\varepsilon)$. The equilibrium loading curve of the CE (1) has a different form in the cases of $\sigma_+ = 0$ or $\sigma_+ > 0$: if $\sigma_+ = 0$, the loading curves family $\sigma(\varepsilon, b)$ converges at $b \rightarrow 0+$ to the straight line $\sigma \equiv 0$ on the entire ray $\varepsilon \geq 0$, and if $\sigma_+ > 0$, it converges to the diagram of an ideal elastoplastic material with a yield stress $\sigma_y = \sigma_+$ and an initial segment of elastic strain $\sigma = f(E\varepsilon)$, $\varepsilon \in [0; \varepsilon_+]$ [8]. Setting $\sigma_+ > 0$ and $V(x) \equiv 0$ at $x \in [0, \sigma_+]$ ensures that the initial segments of all loading curves $\sigma(\varepsilon, b)$ at $\varepsilon \in [0; \varepsilon_+]$ (i.e., at $\sigma \leq \sigma_+$) coincide with the curve $\sigma = f(E\varepsilon)$ (Fig. 5).

All discovered general properties of tensile loading curves are also inherent in compression loading curves, i.e., at $b < 0$ (and $\sigma < 0$): you just need to replace the signs of all inequalities with their inverses and upward convexity with downward convexity, $b \rightarrow 0+$ with $b \rightarrow 0-$, $\sigma_+ \geq 0$ with $\sigma_- \leq 0$, $\varepsilon_+ \geq 0$ with $\varepsilon_- = E^{-1}F(\sigma_-) \leq 0$, the segment $[0; \varepsilon_+]$ with $[\varepsilon_-; 0]$, $[0, \sigma_+]$ with $[\sigma_-; 0]$. The parameter $\sigma_- \leq 0$ (the lower bound of the set of zeros, the MF $V(x)$) has the same physical meaning in compression as σ_+ in tension.

Figure 5 shows the loading curves $\sigma(\varepsilon, b)$ of the model with $\sigma_+ > 0$ and the MF $V(x) \equiv 0$ at $x \in [\sigma_-, \sigma_+]$:

$$\begin{aligned} V &= A_+(x - \sigma_+)^n \text{ at } x > \sigma_+, \\ V &= -A_-|x - \sigma_-|^m \text{ at } x < \sigma_-; \\ F(x) &= x + qV(x), \quad x > 0, \end{aligned} \tag{25}$$

$A_+, A_- > 0$, $m, n \geq 1$, $q \geq 0$ (for any $q \geq 0$ the constraints $F'(x) > 0$ and $F(0) = 0$ are satisfied, since they are satisfied for V). At $\sigma \in [\sigma_-, \sigma_+]$ this model describes a linearly elastic material, and at $\sigma \notin [\sigma_-, \sigma_+]$ rheonic properties and tension-compression asymmetry appear (if $\sigma_- \neq -\sigma_+$ or $A_- \neq A_+$ or $m \neq n$). The loading curve (23) has the following form: $\varepsilon = E^{-1}\sigma$ at $\sigma \in [0, \sigma_+]$, $\varepsilon = E^{-1}[\sigma + qA_+(\sigma - \sigma_+)^n + A_+(n+1)^{-1}(\sigma - \sigma_+)^{n+1}(\tau_r b)^{-1}]$, $\sigma > \sigma_+$.

Figure 5 shows the loading curves of this model with $q = 5$, $\sigma_+ = 0.1$, $n = 2$, $A_+ = 1$, $\eta = 10$, $E = 10$, $\tau_r = 1$ for $b = 10^{i-7}$, $i = 1, \dots, 6$ (curves 1–6). All loading curves have a common straight segment $\sigma = E\varepsilon$, $\varepsilon \leq \varepsilon_+$, $\varepsilon_+ = \sigma_+/E$, independent of rate. At $\sigma > \sigma_+$ the loading curves depend on the rate and shift upward as b increases. At $b \rightarrow 0$ $\sigma(\varepsilon, b) \rightarrow \sigma_+$ for any $\varepsilon \geq \varepsilon_+$, i.e., the loading curves family $\sigma(\varepsilon, b)$ converges to the loading curves of an ideal elastoplastic material with a yield stress $\sigma_y = \sigma_+$ ($\sigma = \sigma_+$ is the straight line 0). The dashed curve ∞ is the limited loading curve at $b \rightarrow \infty$ (since $q > 0$, the instantaneous loading curve is not rectilinear at $\sigma > \sigma_+$). For comparison, the dash-dotted line shows the limiting loading curves at $b \rightarrow \infty$ and $b \rightarrow 0$ for $\sigma_+ = 0.05$ (see the estimate (24)).

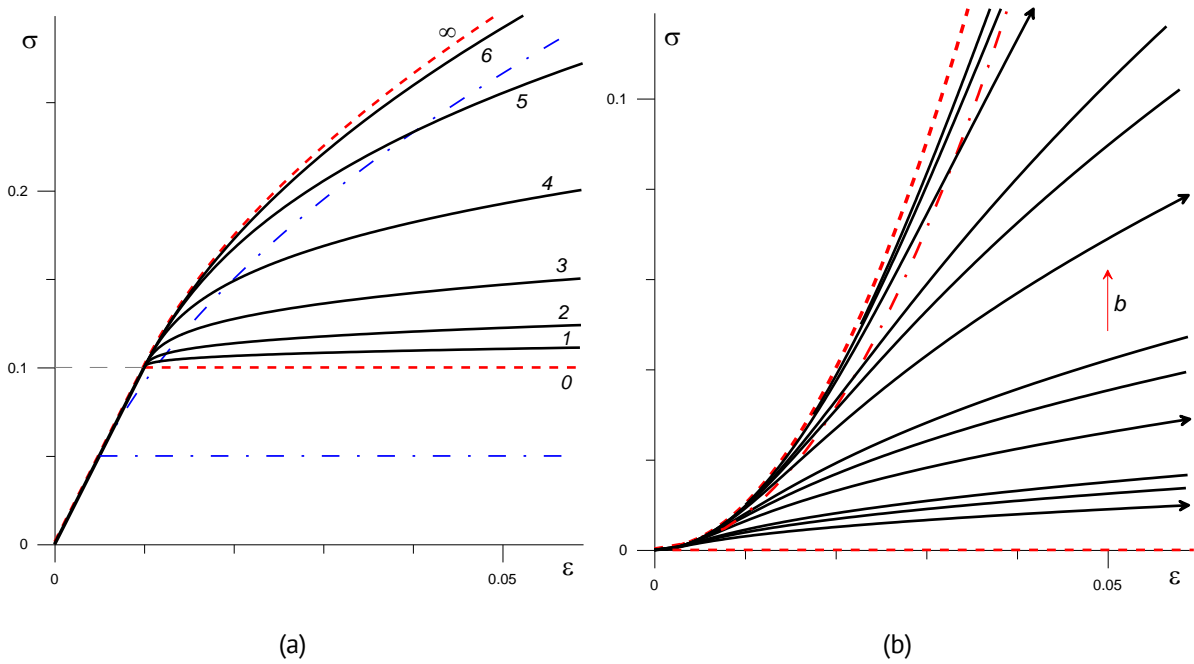


Fig. 5. Different forms of stress-strain curves $\sigma(\varepsilon, b)$, generated by the constitutive equation (1): (a) curves $\sigma(\varepsilon, b)$ generated by the model (25) with $\sigma_+ > 0$ at stress rates $b = 10^{i-7}$, $i = 1, \dots, 6$ (curves 1–6) and limit curves at $b \rightarrow 0+$ or $b \rightarrow \infty$; (dashed lines); (b) stress-strain curves generated by the model (1) with $\sigma_+ = 0$, $\tau_r = 1$, $F = x^{1/2}$ and $V = x$ at stress rates $b = 1 \cdot 10^{-i}$; $2 \cdot 10^{-i}$; $3 \cdot 10^{-i}$, $i = 4; 3; 2; 1$

For the power-law MFs $F = x^m$, $V = x^n$ we have $I(s) = (n + 1)^{-1}s^{n+1}$, and the loading curve (23) takes the form: $\varepsilon(\sigma, b) = E^{-1}\sigma^m + (\gamma b)^{-1}(n + 1)^{-1}\sigma^{n+1}$.

In the case of $n > m - 1 \geq 0$, $F''(x) \geq 0$ and $V(x)$ increases, therefore all loading curves $\sigma(\varepsilon, b)$ with $b > 0$ are convex upward on the semi-axis $\varepsilon > 0$. At $m < 1$ this is not the case: the loading curves have an inflection point and a segment of convexity downwards in the vicinity of zero (see [8] and Fig. 5(b)). Figure 5(b) shows the loading curves $\sigma(\varepsilon, b)$ of the model with $F = x^m$, $V = x^n$, $m = 0.5$, $n = 1$, $\eta = E = 10$, $\tau_r = 1$ for different rates: $b = 1 \cdot 10^{-i}$; $2 \cdot 10^{-i}$; $3 \cdot 10^{-i}$, $i = 4; 3; 2; 1$ (the loading curves $b = 1 \cdot 10^{-i}$ are marked with arrows). The dashed loading curves are the limit curves $\sigma = f(E\varepsilon)$, $f = y^{1/m}$, at $b \rightarrow \infty$ (instantaneous loading curves) and $\sigma = 0$ at $b \rightarrow 0$ (equilibrium loading curve). The dash-dotted curve is the geometric locus of inflection points $(\tilde{\varepsilon}(b), \tilde{\sigma}(b))$ of the loading curves with different $b > 0$; the set $\{(\tilde{\varepsilon}(b), \tilde{\sigma}(b)) | b > 0\}$ does

not depend on η and τ_r , since $\tilde{\sigma}$ and $\tilde{\varepsilon}$ depend only on the parameter $\tau_r b$ [8], and η is included only in it.

Properties of the loading curves with constant rates generated by the CE (4)

The stress-strain curve of the CE (4) is obtained by combining the responses of the CE (1) and the linear CE (3) to the loading $\sigma = bt$, $b > 0$:

$$\varepsilon(\sigma, b) = wE^{-1}[F(\sigma) + (\tau_r b)^{-1}I(\sigma)] + (1 - w)\theta(\sigma/b)\sigma, \quad b, \sigma > 0, \quad (26)$$

where $I(s)$ and $\theta(t)$ are defined in (23) and (18). The equation (26) specifies the stress-strain curves family $\sigma = \sigma(\varepsilon, b)$ of the CE (4) in implicit (inverse) form. The strain (26) increases along σ and decreases along b at $\sigma, b > 0$, and the stress-strain curves family $\sigma = \sigma(\varepsilon, b)$ increases along ε and b . The derivative $\partial\varepsilon/\partial\sigma = wE^{-1}[F'(\sigma) + (\tau_r b)^{-1}V(\sigma)] + (1 - w)\Pi(\sigma/b)$ is positive and decreasing along b at any $\sigma > 0$ (since the CF increases), and at $\sigma = 0$ does not depend on b and the MF V : $\partial\varepsilon/\partial\sigma|_{\sigma=0} = wE^{-1}F'(0) + (1 - w)\Pi(0)$ (and can be equal to 0 or ∞ , if $F'(0) = 0$ or $F'(0) = \infty$). It is obvious that $\varepsilon(0, b) = 0$, and adding the previously proven estimates from below for terms (27) (in particular, $\theta(t) > \theta(0) = \Pi(0)$ [55]), we obtain at any $b, \sigma > 0$ the following estimate:

$$\varepsilon(\sigma, b) > E^{-1}\Phi(\sigma), \quad b, \sigma > 0, \quad \Phi(\sigma) = wF(\sigma) + E(1 - w)\Pi(0)\sigma. \quad (27)$$

(the inequality is strict even at $\sigma < \sigma_+$ in contrast to the inequality for the loading curves of the CE (1)). Since $\Phi(\sigma)$ is an increasing function (and $\Phi(0) = 0$), then there is an inverse function φ , $\varphi(0) = 0$, and for all loading curves in the form $\sigma(\varepsilon, b)$ the estimate from above is valid: $\sigma(\varepsilon, b) < \varphi(E\varepsilon)$ at $b, \varepsilon > 0$ (it does not depend on the MF V). In the case of the model with $F(x) = x$ it has the form $\sigma(\varepsilon, b) \leq [w + E(1 - w)\Pi(0)]^{-1}E\varepsilon$, and in the case of the model with $\Pi(0) = 0$ (as does the CF (5), for example) it has the form $\sigma(\varepsilon, b) \leq f(Ew^{-1}\varepsilon)$, where $f = F^{-1}$.

The stress-strain curves (26) inherit the general properties of the stress-strain curves $\varepsilon(\sigma, b)$, generated by the CE (1) or the CE (3), but they lose some (because the properties of the stress-strain curves of the crossbred CEs are different) and acquire new ones. For arbitrary MFs F , V , Π , subject only to the minimal constraints of one of previous section, and any $w \in (0; 1)$, the following statements are true.

1. The stress-strain curves family (26) increases along σ and decreases along b at $\sigma, b > 0$, and the loading curves family in the form $\sigma = \sigma(\varepsilon, b)$ increases along ε and b , and the estimate $\sigma(\varepsilon, b) < \varphi(E\varepsilon)$ is true at $b, \varepsilon > 0$.
2. If $F''(x) \geq 0$, then $\varepsilon''(\sigma) > 0$, the stress-strain curves (26) are convex downward, and the loading curves $\sigma = \sigma(\varepsilon)$ are convex upward for any b , and if $F''(x) < 0$, then the loading curves $\sigma(\varepsilon, b)$ of the CE (4) can have points of inflection and convexity downward on a certain interval $\varepsilon < \tilde{\varepsilon}(b)$, as well as the stress-strain curves of the CE (1) (in contrast from the CE (3)).
3. The tangent modulus of stress-strain curves $\sigma(\varepsilon, b)$ $\partial\sigma/\partial\varepsilon = [wE^{-1}(F'(\sigma) + (\tau_r b)^{-1}V(\sigma)) + (1 - w)\Pi(\sigma/b)]^{-1}$ increases along b at any $\varepsilon > 0$ (i.e., $\sigma > 0$).
4. Instantaneous modulus of stress-strain curves $\sigma(\varepsilon, b)$ (limit of the tangent modulus at $\varepsilon \rightarrow 0+$) $G = [wE^{-1}F'(0) + (1 - w)\Pi(0)]^{-1}$ does not depend on the rate b and MF V (and can be equal to 0 or ∞).
5. At $b \rightarrow \infty$ $\theta(\sigma/b) \rightarrow \theta(0+) = \Pi(0)$ the stress-strain curves family (26) also converges

to the function $E^{-1}\Phi(\sigma)$ on the ray $\sigma \geq 0$ (see (27)). Therefore the loading curves family in the form $\sigma(\varepsilon, b)$ converges at $b \rightarrow \infty$ to the inverse function $\varphi(E\varepsilon)$ on the semi-axes $\varepsilon \geq 0$, i.e., the curve $\sigma = \varphi(E\varepsilon)$ is the instantaneous loading curve of the CE (4) (it does not depend on the MF V , in particular, on the material parameter σ_+ , and on the CF $\Pi(t)$, because in the definition of $\Phi(\sigma)$ only the initial value $\Pi(0)$ is included). It is easy to check that the convergence is uniform on any segment of the ε axis.

6. If $\Pi(0) = 0$, then $\Phi(\sigma) = wF(\sigma)$, $\varphi(\varepsilon) = f(\varepsilon/w)$ and the instantaneous stress-strain curve has the form $\sigma = f(Ew^{-1}\varepsilon)$, i.e., is obtained from the loading curves of the CE (1) by tension along the ε axis with a coefficient w . In contrast to the linear CE (3), it does not degenerate into a vertical straight line $\varepsilon = 0$, if $\Pi(0) = 0$. That is adding the CE (1) with any weighting factor $w > 0$ (arbitrarily small) to the singular linear model produces its regularization. This can also be seen from the formula for the instantaneous modulus G , which no longer goes to infinity in the case of $\Pi(0) = 0$ (provided that $F'(0) \neq 0$).

7. If $\sigma_+ = 0$, then for any $\sigma > 0$ from (26) follows $\varepsilon(\sigma, b) \rightarrow \infty$ at $b \rightarrow 0+$, and the stress-strain curves family $\sigma = \sigma(\varepsilon, b)$ converges at $b \rightarrow 0+$ (and $\varepsilon = \text{const}$) to the function $\sigma \equiv 0$ on the entire ray $\varepsilon \geq 0$. The first is obvious (since $I(\sigma) > 0$ at $\sigma > 0$, and $b^{-1} \rightarrow \infty$), and to prove the second we need to fix $\varepsilon = \bar{\varepsilon} = \text{const}$ in (26) and go to the limit $b \rightarrow 0+$: assuming that $\sigma(\varepsilon, b) \rightarrow \sigma_*$, $\sigma_* > 0$, we obtain that the first term in (26) has a finite limit $wE^{-1}F(\sigma_*)$, the third term has a limit $(1-w)\theta(\infty)\sigma_* = (1-w)\Pi(\infty)\sigma_*$, which can be finite at $\Pi(\infty) < \infty$, and the second term is $wE^{-1}(\tau_r b)^{-1}I(\sigma_*) \rightarrow \infty$, and therefore the entire sum tends to infinity, which contradicts the finiteness of the left side of (26). Therefore, the assumption $\sigma_* > 0$ is untrue and $\sigma_* = 0$ for any $\varepsilon \geq 0$. For models with $\sigma_+ > 0$ the equilibrium diagram may differ from $\sigma \equiv 0$.

8. If $\sigma_+ > 0$ in the MF of the CE (4), then $I(\sigma) \equiv 0$ at $\sigma \leq \sigma_+$, and therefore the stress-strain curve (26) has the following form:

$$\varepsilon(\sigma, b) = wE^{-1}F(\sigma) + (1-w)\theta(\sigma/b)\sigma, \sigma \leq \sigma_+, b > 0, \quad (28)$$

that is, in contrast with the CE (1) (case $w = 1$) the stress-strain curve depends on the rate at $\sigma \leq \sigma_+$ (Fig. 6(a)) also. Since $\Pi(0) < \theta(t) < \Pi(\infty)$ [55], then at $\Pi(\infty) < \infty$ (i.e. $G_\infty > 0$) the two-sided estimate is true: $E^{-1}\Phi(\sigma) < \varepsilon(\sigma, b) < E^{-1}\Phi_\infty(\sigma)$, $\sigma \leq \sigma_+$, $b > 0$, $\Phi_\infty(\sigma) = wF(\sigma) + E(1-w)\Pi(\infty)\sigma$. Since $\Phi(\sigma)$ and $\Phi_\infty(\sigma)$ are the increasing functions, then applying to the inequalities the inverse functions $\varphi = \Phi^{-1}$ and $\varphi_\infty = \Phi_\infty^{-1}$ ($\varphi(0) = 0$ and $\varphi_\infty(0) = 0$, because $\Phi(0) = 0$, $\Phi_\infty(0) = 0$), we obtain an estimate for the loading curves (29) in the form $\sigma = \sigma(\varepsilon, b)$: $\varphi_\infty(E\varepsilon) < \sigma(\varepsilon, b) < \varphi(E\varepsilon)$ at $\varepsilon \leq \bar{\varepsilon}_+(b)$, $b > 0$, where $\bar{\varepsilon}_+(b) = \varepsilon(\sigma_+, b) = wE^{-1}F(\sigma_+) + (1-w)\theta(\sigma_+/b)\sigma_+$ (the strain value corresponding to the stress $\sigma = \sigma_+$ now depends on the loading rate in contrast to the value $\varepsilon_+ = F(\sigma_+)/E$ in the CE (1)). The function $\bar{\varepsilon}_+(b)$ decreases monotonically (since $\theta(t)$ increases) and $\bar{\varepsilon}_+(b) \rightarrow \hat{\varepsilon}$ at $b \rightarrow 0+$ (fig. 6a), where:

$$\hat{\varepsilon} = \varepsilon(\sigma_+, \infty) = wE^{-1}F(\sigma_+) + (1-w)\Pi(\infty)\sigma_+ = E^{-1}\Phi_\infty(\sigma_+). \quad (29)$$

9. For models with $\sigma_+ > 0$ and $\Pi(\infty) < \infty$ (Fig. 6(a)) the loading curves family (28) at $b \rightarrow 0+$ has a limit $E^{-1}\Phi_\infty(\sigma)$ at all $\sigma \leq \sigma_+$ (since $\theta(\infty) = \Pi(\infty)$ [55]), $\hat{\varepsilon} < \infty$ and the stress-strain curves family $\sigma(\varepsilon, b)$, $\varepsilon \leq \bar{\varepsilon}_+(b)$, converges to the function $\sigma = \varphi_\infty(E\varepsilon)$, $\varepsilon \in [0; \hat{\varepsilon}]$, i.e., the equilibrium stress-strain curve increases.

10. For models with $\sigma_+ > 0$ and $\Pi(\infty) = \infty$ (Fig. 6(b)) $\varepsilon(\sigma, b) \rightarrow \infty$, $\hat{\varepsilon} = \infty$ and the stress-strain curves family $\sigma(\varepsilon, b)$ converges to the function $\sigma \equiv 0$ at all $\varepsilon \geq 0$, i.e. the equilibrium stress-strain curve is the same as in the case of $\sigma_+ = 0$.

11. For models with $\sigma_+ > 0$ and $\Pi(\infty) < \infty$ the equilibrium curve at $\sigma > \sigma_+$, i.e., at $\varepsilon > \hat{\varepsilon}$, coincide with the straight line $\sigma = \sigma_+$ (and at $\varepsilon \in [0; \hat{\varepsilon}]$ has a form $\sigma = \varphi_\infty(E\varepsilon)$, as proven above). The proof is similar to the proof of property 7: the assumption $\sigma_* > \sigma_+$ leads to a contradiction, and therefore $\sigma_* = \sigma_+$ (only then $I(\sigma_*) = 0$, the second term in the limit of the right side of (26) vanishes, and it has a finite limit, since this is true for the third term due to the condition $\Pi(\infty) < \infty$).

Figure 6(a) shows the stress-strain curves of three CE (4) with the same material parameters and MFs (25) as in Fig. 5(a) ($\sigma_+ = 0.1, E = 10, \tau_r = 1$), and the CFs in the form (6) with the same parameters as in Fig. 4(a) ($\lambda = 0.1, \beta = 1, \gamma = 0.9, G = 10, G_\infty = 1$, retardation time $\tau = 1/\lambda = 10$, relaxation time $\tilde{\tau}_r = 1$), with three different weighting factors $w = 1; 0.5; 0$ (light blue, black and blue curves) for six rates $b = 10^{i-6}, i = 1, \dots, 6$ (curves 1–6). The light blue stress-strain curves 1'–5' (for $w = 1$) coincide with the stress-strain curves of the CE (1) in Fig. 5(a) (they have a common straight segment OA, independent of the rate: $\sigma = E\varepsilon, \varepsilon \leq \varepsilon_+, \varepsilon_+ = \sigma_+/E$), the blue stress-strain curves 3''–6'' (for $w = 0$ and $b = 0.001; 0.01; 0.1; 1$) coincide with the loading curves of the linear Kelvin model in Fig. 4(a) (stress-strain curves 1'', 2'' at lower rates merge with the equilibrium loading curve 0''), dash-dotted blue straight lines 0'' and ∞'' are the limit stress-strain curves at $b \rightarrow 0$ and $b \rightarrow \infty$ from the estimate (20), the dashed red curves 0' and ∞' – are the limit stress-strain curves for CE (1) (the same as in fig. 5a), the dash-dotted red curve ∞ is the limit stress-strain curve $\sigma = \varphi(E\varepsilon), \varepsilon \geq 0$, of the CE (4) at $b \rightarrow \infty$. At $b \rightarrow 0$ $\sigma(\varepsilon, b) \rightarrow \sigma_+$ for any $\varepsilon \geq \hat{\varepsilon}$, in our example $\Pi(\infty) < \infty, 0 < G_\infty < E$ and $\hat{\varepsilon} = 0.055$; for models with $G_\infty > \sigma_+/\varepsilon_+ = E\sigma_+/F(\sigma_+)$ it will be $\hat{\varepsilon} < \varepsilon_+$). On the segment $[0; \hat{\varepsilon}]$ the stress-strain curves family of the CE (4) $\sigma(\varepsilon, b)$ converges at $b \rightarrow 0$ to the linear function (since the MF F is linear and $\Pi(\infty) < \infty$), the graph of which is the segment OB, $B(\hat{\varepsilon}, \sigma_+)$.

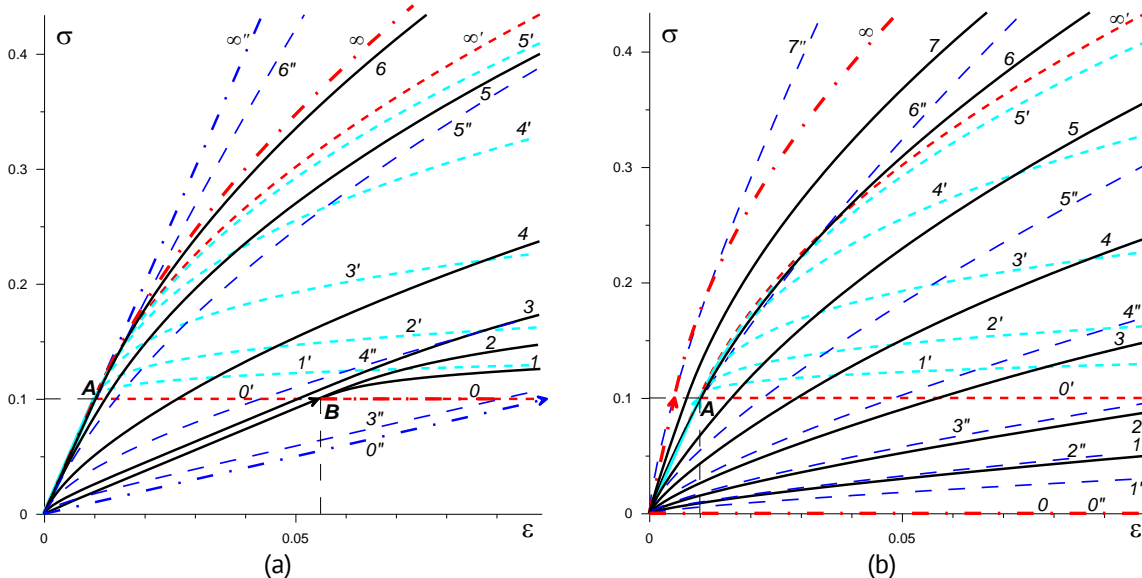


Fig. 6. Stress-strain curves $\sigma(\varepsilon, b)$ generated by the constitutive equation (4) with the same material functions (25) as in the Fig. 5(a) for three different weighting factors $w = 0; 0.5; 1$ (light blue, black, and blue curves) at stress rates $b = 10^{i-6}, i = 1, \dots, 7$: (a) crossbreed of the model (1) and the standard linear solid model (6) (with the same material parameters as in the Fig. 4(a)); (b) crossbreed of the model (1) and the fractional model (5) with $u = 0.3, A = 0.3$

Figure 6(b) shows the stress-strain curves of three CE (4) with the same material parameters and MFs (25) as in Fig. 5(a) ($\sigma_+ = 0.1$, $E = 10$, $\tau_r = 1$), but with power-law CFs (5) with $u = 0.3$, $A = 0.3$, with three different weighting factors $w = 1; 0.5; 0$ (light blue, black and blue curves) for seven rates $b = 10^{i-6}$, $i = 1, \dots, 7$ (curves $1'-5'$, $1-7$, $1''-7''$). The light blue stress-strain curves $1'-5'$ (for $w = 1$) coincide with the stress-strain curves of the CE (1) in Figs. 5(a) and 6(a) (they have a common straight segment OA , independent of the rate: $\sigma = E\varepsilon$), the dashed red curves $0'$ and ∞' are the limit loading curves at $b \rightarrow 0$ and $b \rightarrow \infty$ (the same as in Fig. 6(a)). The blue stress-strain curves $2''-6''$ (for $w = 0$ and $b = 0.0001; 0.001; 0.01; 0.1; 1$) coincide with stress-strain curves $0-4$ of the linear fractal model (5) in Fig. 4(b); it is irregular, $\Pi(0) = 0$, $G = \infty$, $\Pi(\infty) = \infty$, $G_\infty = 0$, at $b \rightarrow 0$ its stress-strain curves family (22) $\sigma(\varepsilon, b)$ converges to the function $\sigma \equiv 0$, as at $b \rightarrow \infty$ the family $\varepsilon(\sigma, b)$ converges to $\varepsilon = 0$, i.e., the stress-strain curves $\sigma(\varepsilon, b)$ converge to the vertical semi-axis. For this reason, at $b \rightarrow 0$ the stress-strain curves family of the CE (4) with $w \in (0; 1)$ (see the black loading curves $1-7$) converges to the function $\sigma = 0$ on the entire semi-axis $\varepsilon \geq 0$ (property 10), and at $b \rightarrow \infty$ converges to the function $\sigma = \varphi(E\varepsilon) = f(Ew^{-1}\varepsilon)$, $\varepsilon \geq 0$, $f = F^{-1}$ (the dash-dotted red curve ∞), since according to (27) $\Phi(\sigma) = wF(\sigma)$.

If the value of $w - 1$ is sufficiently small, then the contribution of the last term to the strain (26) is negligible, the properties of the loading curves (26) coincide with the properties of the stress-strain curves (23) of the CE (1) with the exception of two qualitative differences:

1. for models with $\sigma_+ > 0$ at any $w \neq 1$ the stress-strain curve (26) depends on the loading rate even in the range $\sigma \in [0; \sigma_+]$ (see (28)), in which $V(x) \equiv 0$ and $I(\sigma) \equiv 0$, although this dependence is weakly expressed if the material parameter w is close to one;
2. the equilibrium stress-strain curve for $w \neq 1$ can differ qualitatively from the limiting case $w = 1$ (Fig. 6(b)) and has a different form in the cases $\sigma_+ = 0$ or $\sigma_+ > 0$, and in the latter case the key role is played by the limited or unbounded nature of the CF $\Pi(t)$ (see properties of loading curves 7-11): for the models with $\sigma_+ = 0$ or with $\sigma_+ > 0$ and $\Pi(\infty) = \infty$ (Fig. 6(b)), the equilibrium curve has a form $\sigma \equiv 0$ on the entire ray $\varepsilon \geq 0$, and for the models with $\sigma_+ > 0$ and $\Pi(\infty) < \infty$ (Fig. 6(a)) the value (29) is finite and the equilibrium curve is non-zero: $\sigma = \varphi_\infty(E\varepsilon)$ at $\varepsilon \in [0; \hat{\varepsilon}]$ and $\sigma = \sigma_+$ at $\varepsilon > \hat{\varepsilon}$.

Conclusion

The paper formulates a generalization (4), (10) of the physically nonlinear CE of Maxwell-type viscoelastoplasticity (1), (7) with four MFs (two MFs in the uniaxial case (4)), the general properties, the arsenal of possibilities, and the scope of applicability of which have been studied earlier in a series of articles by the author [4–10]. In order to generalize the CE (1), (7), preserving its advantages, but eliminating the detected disadvantages that reduce its applicability, and to expand the range of rheological effects it describes, it is proposed to add a third (viscoelastic) strain component to the CE (1), (7), a term expressed by the linear integral Boltzmann–Volterra operator (3), (8) with arbitrary CF. For generality and convenience of model control, for its adjustment for different materials and lists of simulated effects, in addition to the three MFs, a weighting factor $w \in [0; 1]$ (degree of nonlinearity) is introduced into the CE (4), which allows “mixing” the nonlinear

CE (1), (7) and the linear viscoelasticity operator (3), (8) in arbitrary proportions and regulate the severity of different sets of effects modeled by them. Thus, the CE (4), (10) is a hybrid (and simultaneous generalization) of the CE (1), (7) and the linear viscoelasticity CE (3), (8) (at $w = 0$ nonlinearity is switched off, and the linear viscoelasticity CE is obtained, and at $w = 1$ the nonlinear CE (1) is obtained). The proposed CE allows not only to expand the scope of applicability of the CE (1), (7), but also to connect the nonlinear viscoplasticity model (1), (7) to the linear viscoelasticity CE (3), (8), and to surgically adjust this connection depending on the characteristics of the testing data of a particular material: thanks to the choice of two material parameters σ_+ and w , nonlinear viscoplasticity can be added, starting from any stress $\sigma \geq \sigma_+ > 0$ and in any proportion.

The equations for the creep and recovery curves families and constant-rate loading curves generated by the proposed CE (4) with three arbitrary MFs are derived, their general properties and the influence of loading parameters and characteristics of all MFs on them are analytically studied and compared with the properties of the creep and stress-strain curves of crossbred CEs (1) and (3). In particular, new qualitative properties (effects) are identified that make it possible to describe the more general CE (4) in comparison with the original CE (1). It is verified that the generalization eliminates a number of disadvantages of the CE (1), but retains its valuable qualities (4–8). For example:

1. the CE (4) makes it possible to describe not only creep at a constant rate, as the CE (1), but also creep at a variable rate, as well as limited creep, characteristic, for example, of many polymers;
2. the CE (4) describes the recovery after complete unloading ("reverse creep") with a gradual yielding of strain to a certain constant level at large values of times;
3. the possibilities for describing the various properties of the stress-strain curves families, in particular the forms of equilibrium and instantaneous loading curves, are significantly expanded;
4. adding the CE (1) with any weighting factor $w > 0$ (arbitrarily small) to any singular linear model of the form (3), (8) produces its regularization (in particular, the instantaneous modulus no longer goes to infinity in the case of $\Pi(0) = 0$, and such a model appears with an instantaneous loading curve instead of a limiting vertical straight line at $b \rightarrow \infty$ [55,56]).

Thus, the performed primary analysis showed that the proposed more general CE (4), (7) provides many opportunities for describing the various properties of stress-strain curves and creep and recovery curves of materials (for adjusting their shape and tuning them to testing data). It also allows expanding significantly the range of described rheological effects and the range of applicability of the Maxwell-type viscoelastoplasticity relation and deserves further research and application in modeling. In the following papers, the properties found will be used to develop methods for identifying the CE (4), (7) from the loading and creep curves and recovery curve of materials, as was done for the CE (1), (7) in [5,7–10,56].

References

1. Khokhlov AV. Two-sided estimates for the relaxation function of the linear theory of heredity via the relaxation curves during the ramp-deformation and the methodology of identification. *Mechanics of Solids*. 2018; 53(3): 307–328.
2. Khokhlov AV. Analysis of properties of ramp stress relaxation curves produced by the Rabotnov non-linear hereditary theory. *Mechanics of Composite Materials*. 2018;54(4): 473–486.
3. Khokhlov AV. Properties of the Set of Strain Diagrams Produced by Rabotnov Nonlinear Equation for Rheonomous Materials. *Mechanics of Solids*. 2019;54(3): 384–399.
4. Khokhlov AV. Long-term strength curves generated by the nonlinear Maxwell-type model for viscoelastoplastic materials and the linear damage rule under step loading. *Journal of Samara State Technical University, Ser. Physical and Mathematical Sciences*. 2016;20(3): 524–543.
5. Khokhlov AV. The nonlinear Maxwell-type model for viscoelastoplastic materials: Simulation of temperature influence on creep, relaxation and strain-stress curves. *The Journal of Samara State Technical University, Ser. Physical and Mathematical Sciences*. 2017;21(1): 160–179. [In Russian]
6. Khokhlov AV. A Nonlinear Maxwell-Type Model for Rheonomic Materials: Stability under Symmetric Cyclic Loadings. *Moscow University Mechanics Bulletin*. 2018;73(2): 39–42.
7. Khokhlov AV. Applicability Indicators and Identification Techniques for a Nonlinear Maxwell-Type Elasto-Viscoplastic Model using Multi-Step Creep Curves. *Herald of the Bauman Moscow State Technical University. Series Natural Sciences*. 2018(6): 92–112. [In Russian]
8. Khokhlov AV. Applicability indicators and identification techniques for a nonlinear Maxwell-type elastoviscoplastic model using loading–unloading curves. *Mechanics of Composite Materials*. 2019;55(2): 195–210.
9. Khokhlov AV. Possibility to Describe the Alternating and Non-monotonic Time Dependence of Poisson's Ratio during Creep Using a Nonlinear Maxwell-Type Viscoelastoplasticity Model. *Russian Metallurgy (Metally)*. 2019;10: 956–963.
10. Khokhlov AV, Shaporev AV, Stolyarov ON. Loading-unloading-recovery curves for polyester yarns and identification of the nonlinear Maxwell-type viscoelastoplastic model. *Mechanics of Composite Materials*. 2023;59(1): 129–146.
11. Rabotnov YuN. *Creep Problems in Structural Members*. Moscow: Nauka; 1966. [In Russian]
12. Bugakov II. *Creep of polymer materials*. Moscow: Nauka; 1973. [In Russian]
13. Malinin NN. *Creep design of engineering structures*. Moscow: Mashinostroenie Publ.; 1981. [In Russian]
14. Gokhfel'd DA, Sadakov OS. *Plasticity and creep in structural elements under repeated loading*. Moscow: Mashinostroenie Publ.; 1984. [In Russian]
15. Nikitenko AF. *Creep and long-term strength of metallic materials*. Novosibirsk: NGASU; 1997. [In Russian]
16. Betten J. *Creep Mechanics*. Berlin: Springer; 2008.
17. Lokoshchenko AM. *Creep and long-term strength of metals*. Moscow: Fizmatlit Publ.; 2016. [In Russian]
18. Lakes RS. *Viscoelastic Materials*. Cambridge: Cambridge Univ. Press; 2009.
19. Bergstrom JS. *Mechanics of Solid Polymers. Theory and Computational Modeling*. Elsevier; 2015.
20. Vinogradov GV, Malkin AYa. *Polymer rheology*. Moscow: Khimiya Publ.; 1977. [In Russian]
21. Larson RG. *Constitutive Equations for Polymer Melts and Solutions*. Butterworth: Boston; 1988.
22. Gupta RK. *Polymer and composite rheology*. NY: Marcel Dekker; 2000.
23. Malkin AY, Isayev AI. *Rheology: Conceptions, methods, applications*. 2-nd Ed. Toronto: ChemTec Publishing; 2012.
24. Brinson HF, Brinson LC. *Polymer Engineering Science and Viscoelasticity*. Springer; 2008.
25. Kalinnikov AE, Vakhrushev AV. Creep of materials of different tensile and compressive strengths under variable loads. *Mechanics of Composite Materials*. 1982;18(3): 267–272.
26. Fatemi A, Yang L. Cumulative fatigue damage and life prediction theories: A survey of the state of the art for homogeneous materials. *International Journal of Fatigue*. 1998;20(1): 9–34.
27. Launay A, Maitournam MH, Marco Y, Raoult I, Szymtka F. Cyclic behaviour of short glass fibre reinforced polyamide: Experimental study and constitutive equations. *International Journal of Plasticity*. 2011;27(8): 1267–1293.
28. Darabi MK, Al-Rub RKA, Masad EA, Huang CW, Little DN. A modified viscoplastic model to predict the permanent deformation of asphaltic materials under cyclic-compression loading at high temperatures. *International Journal of Plasticity*. 2012;35: 100–134.
29. Takagi H, Dao M, Fujiwara M. Prediction of the Constitutive Equation for Uniaxial Creep of a Power-Law Material through Instrumented Microindentation. *Testing and Modeling. Materials Transactions*. 2014;55(2): 275–284.
30. Chinh NQ, Szommer P. Mathematical description of indentation creep and its application for the determination of strain rate sensitivity. *Materials Science & Engineering A*. 2014;611: 333–336.

31. Petukhov DS, Keller IE. Dual plane problems for creeping flows of power-law incompressible medium. *The Journal of Samara State Technical University, Ser. Physical and Mathematical Sciences*. 2016;20(3): 496–507. [In Russian]
32. Kaibishev OA. *Superplasticity of industrial alloys*. Moscow: Metallurgiya Publ.; 1984. [In Russian]
33. Nieh TG, Wadsworth J, Sherby OD. *Superplasticity in metals and ceramics*. Cambridge Univ. Press; 1997.
34. Padmanabhan KA, Vasin RA, Enikeev FU. *Superplastic Flow: Phenomenology and Mechanics*. Berlin: Springer; 2001.
35. Segal VM, Beyerlein IJ, Tome CN, Chuvil'deev VN, Kopylov VI. *Fundamentals and Engineering of Severe Plastic Deformation*. NY: Nova Science Pub. Inc.; 2010.
36. Zhilayev AP, Pshenichnyuk AI. *Superplasticity and grain boundaries in ultrafine-grained materials*. Cambridge: Cambridge Intern. Sci. Publ.; 2010.
37. Cao Y. Determination of the creep exponent of a power-law creep solid using indentation tests. *Mechanics of Time-Dependent Materials*. 2007;11: 159–172.
38. Megahed M, Ponter ARS, Morrison CJ. An experimental and theoretical investigation into the creep properties of a simple structure of 316 stainless steel. *International Journal of Mechanical Sciences*. 1984;26(3): 149–164.
39. Enikeev FU. Experimental evaluation of speed sensitivity of superplastic material in strongly non-uniform deflected mode. *Industrial Laboratory. Diagnostics of Materials*. 2007;73(10): 44–50. [In Russian]
40. Mochugovskiy AG, Mosleh AO, Kotov AD, Khokhlov AV, Kaplanskaya LY, Mikhaylovskaya AV. Microstructure Evolution, Constitutive Modelling, and Superplastic Forming of Experimental 6XXX-Type Alloys Processed with Different Thermomechanical Treatments. *Materials*. 2023;16(1): 445.
41. Eglit ME, Yakubenko AE, Zayko JS. Mathematical Modeling of Slope Flows of Non-Newtonian Media. *Proceedings of the Steklov Institute of Mathematics*. 2018;300: 219–229.
42. Radchenko VP, Shapievsii DV. Mathematical creep model for micro-nonhomogeneous non-linear elastic material. *Prikladnaya mekhanika I tekhnicheskaya fizika*. 2008;49(3): 157–163. [In Russian]
43. Naumenko K, Altenbach H, Gorash Y. Creep Analysis with a Stress Range Dependent Constitutive Model. *Archive of Applied Mechanics*. 2009;79: 619–630.
44. Lu LY, Lin GL, Shih MH. An experimental study on a generalized Maxwell model for nonlinear viscoelastic dampers used in seismic isolation. *Engineering Structures*. 2012;34(1): 111–123.
45. Monsia MD. A Simplified Nonlinear Generalized Maxwell Model for Predicting the Time Dependent Behavior of Viscoelastic Materials. *World Journal of Mechanics*. 2011;1: 158–167.
46. Stolin AM, Khokhlov AV. Nonlinear model of shear flow of thixotropic viscoelastoplastic continua taking into account the evolution of the structure and its analysis. *Moscow University Mechanics Bulletin*. 2022;77(5): 127–135.
47. Khokhlov AV, Gulin VV. Analysis of the nonlinear Maxwell-type constitutive equation for shear flow of thixotropic viscoelastic media accounting for interaction of deformation process and structure evolution. *Physical Mesomechanics*. 2023;26(6): 621–642.
48. Gorodtsov VA, Leonov AI. On the kinematics, nonequilibrium thermodynamics, and rheological relationships in the nonlinear theory of viscoelasticity. *Journal of Applied Mathematics and Mechanics*. 1968;32(1): 62–84.
49. Leonov AI, Lipkina ECh, Paskhin ED, Prokunin AN. Theoretical and experimental investigations of shearing in elastic polymer liquids. *Rheologica Acta*. 1976;15(7/8): 411–426.
50. Pal'mov VA. Rheological models in the nonlinear mechanics of deformable bodies. *Uspekhi mekhaniki*. 1980;3(3): 75–115. [In Russian]
51. Prokunin AN. On the non-linear Maxwell-type defining equations for describing the motions of polymer liquids. *Journal of Applied Mathematics and Mechanics*. 1984;48(6): 699–706.
52. Leonov AI, Prokunin AN. *Non-linear Phenomena in Flows of Viscoelastic Polymer Fluids*. London: Chapman and Hall; 1994.
53. Leonov AI. Constitutive equations for viscoelastic liquids: Formulation, analysis and comparison with data. *Rheology Series*. 1999;8: 519–575.
54. Khokhlov AV. Analysis of creep curves produced by the linear viscoelasticity theory under cyclic stepwise loadings. *The Journal of Samara State Technical University, Ser. Physical and Mathematical Sciences*. 2017;21(2): 326–361. [In Russian]
55. Khokhlov AV. Specific features of stress-strain curves at constant stress rate or strain rate yielding from linear viscoelasticity. *Problems of Strength and Plasticity*. 2015;77(2): 139–154. [In Russian]
56. Khokhlov AV. Analysis of the bulk creep influence on stress-strain curves under tensile loadings at constant rates and on Poisson's ratio evolution based on the linear viscoelasticity theory. *The Journal of Samara State Technical University, Ser. Physical and Mathematical Sciences*. 2019;23(4): 671–704. [In Russian]
57. Krishtal MM. Instability and mesoscopic inhomogeneity of plastic deformation (analytical review). Part I. Phenomenology of the sharp yield point and jerky flow. *Physical Mesomechanics*. 2004;7(5–6): 5–26.
58. Rudskoi AM, Rudaev Yal. *Mechanics of dynamic superplasticity of aluminum alloys*. St. Petersburg: Nauka; 2009. [In Russian]

59. Yu D, Chen X, Yu W, Chen G. Thermo-viscoplastic modeling incorporating dynamic strain aging effect on the uniaxial behavior of Z2CND18.12N stainless steel. *International Journal of Plasticity*. 2012;37: 119–139.
60. Trusov PV, Chechulina EA. Serrated yielding: physical mechanisms, experimental dates, macro-phenomenological models. *PNRPU Mechanics Bulletin*. 2014;(3): 186–232. [In Russian]
61. Lin YC, Chen XM. A critical review of experimental results and constitutive descriptions for metals and alloys in hot working. *Materials and Design*. 2011;32(4): 1733–1759.
62. McClung AJW, Ruggles-Wrenn MB. The rate (time)-dependent mechanical behavior of the PMR-15 thermoset polymer at elevated temperature. *Polymer Testing*. 2008;27(7): 908–914.
63. Kastner M, Obst M, Brummund J, Thielsch K, Ulbricht V. Inelastic material behavior of polymers – Experimental characterization, formulation and implementation of a material model. *Mechanics of Materials*. 2012;52: 40–57.
64. Yun KS, Park JB, Jung GD, Youn SK. Viscoelastic constitutive modelling of solid propellant with damage. *International Journal of Solids and Structures*. 2016;80: 118–127.
65. Fung YC. *Biomechanics. Mechanical Properties of Living Tissues*. New York: Springer; 1993.
66. Diani J, Fayolle B, Gilormini P. A review on the Mullins effect. *European Polymer Journal*. 2009;45(3): 601–612.
67. Zhu Y, Kang G, Yu C, Poh LH. Logarithmic rate based elasto-viscoplastic cyclic constitutive model for soft biological tissues. *Journal of Mechanical Behavior of Biomedical Materials*. 2016;61: 397–409.
68. Qi H, Boyce M. Stress-strain behavior of thermoplastic polyurethanes. *Mechanics of Materials*. 2005;37(8): 817–839.
69. Drozdov AD, Dusunceli N. Unusual mechanical response of carbon black-filled thermoplastic elastomers. *Mechanics of Materials*. 2014;69(1): 116–131.

About the Author

Andrew V. Khokhlov  

Ph. D. in Technical Sciences

Senior Researcher (Institute of Mechanics, Lomonosov Moscow State University, Moscow, Russia)

Associate Professor (Department of Composites Mechanics, Faculty of Mechanics and Mathematics, Lomonosov Moscow State University, Moscow, Russia)

Leading Researcher (Laboratory "Polymer composites for the North", North-Eastern Federal University, Yakutsk, Russia)